Mechanical Systems and Signal Processing 224 (2025) 112089

Contents lists available at ScienceDirect

Mechanical Systems and Signal Processing

journal homepage: www.elsevier.com/locate/ymssp

In-vacuo adaptive beam element for vibration control

P. Gardonio [a,*], E. Rustighi [b], S. Baldini [a], C. Malacarne [c], M. Perini [c]

[a] Università degli Studi di Udine, Dipartimento Politecnico di Ingegneria e Architettura, Italy
[b] Università degli Studi di Trento, Dipartimento Ingegneria Industriale, Italy
[c] ProM Facility, Trentino Sviluppo S.p.A., Italy

ARTICLE INFO

Keywords:
Adaptive structure
Adaptive material
Structured fabric
Chain mail fabric
In-vacuo fabric
Granular material
Jamming transition
Adaptive tuneable vibration absorber

ABSTRACT

This paper proposes a novel in-vacuo adaptive beam element for vibration control, which, in this study, is employed as an adaptive tuneable vibration absorber. The element is formed by a composite beam with a core of structured fabrics wrapped in a deflated plastic bag skin. The fabrics consist of 3D-printed chain mails of hollowed truss-like particles. A base post is connected at the middle section of the composite beam, such that its flexural vibration is controlled by a flapping fundamental natural mode whose natural frequency can be varied by changing the vacuum level in the bag. The dynamics of this arrangement replicates that of a suspended mass-spring-damper system and, thus, can be suitably used as a tuneable vibration absorber. The study considers in-vacuo composite beams with one or two overlapping chain mails made with cubic, spherical-octahedral, octahedral hollowed truss-like particles. To start with, the dynamic response of these structures is analysed with respect to dynamic stiffness frequency response functions measured with a six-point bending setup. The dynamic response of the centrally pinned in-vacuo adaptive beam element is then investigated considering the vibration transmissibility and base impedance frequency response functions. Finally, the tuning features and vibration control effects of the adaptive beam element are assessed by fitting it at the free termination of a clamped beam in order to control the resonant response of a target flexural mode. Overall, the experimental results have shown that the fundamental natural frequency of the proposed in-vacuo adaptive beam element can be swiftly lifted or lowered by modulating the vacuum level in the bag encasing the structured fabrics. Indicatively, the working centre frequency of the resulting absorber depends on the number of strips piled in the vacuum bag, which defines the thickness, and thus the reference bending stiffness, of the in-vacuo composite beam. Also, the working frequency bandwidth of the in-vacuo adaptive beam element mostly depends on the geometry, the material and the finishing of the chain mail particles. In fact, these properties infer on the number, the type (between convex or non-convex surfaces), the area and the friction coefficient of the contacts that develop between neighbouring particles of the mails and thus determine the range of bending stiffness that can be achieved by a given vacuum range in the deflated bag.

1. Introduction

Controlling vibration at low audio frequencies with classical passive treatments is a challenging problem, primarily because it

* Corresponding author.
E-mail address: paolo.gardonio@uniud.it (P. Gardonio).

https://doi.org/10.1016/j.ymssp.2024.112089
Received 26 July 2024; Accepted 22 October 2024
Available online 4 November 2024
0888-3270/© 2024 The Authors. Published by Elsevier Ltd. This is an open access article under the CC BY-NC-ND license (http://creativecommons.org/licenses/by-nc-nd/4.0/).

would require either bulky mass, stiffness, damping treatments or optimally designed vibration isolators and Tuned Vibration Absorbers (TVA) [1–4]. Moreover, passive treatments work well at nominal operation conditions and cannot adapt to changes of either the disturbance or the dynamic response of the hosting structure. For this reason, the past three decades have seen a growing interest in Adaptive Tuned Vibration Absorbers (ATVA), which can be effectively adopted either to control low frequency time-harmonic vibrations of mechanical systems subject to variable tonal excitations or to mitigate the low frequency resonant responses of time-varying distributed structures subject to broadband stationary stochastic disturbances [5]. Normally, ATVA systems rely on electro-mechanical solutions to create a tuneable spring-mass-damper system, such as, for example, shape memory alloys [6–9], magneto-rheological and electrorheological elastomers [10–14], thermo-viscoelastic materials [15,16], geometric regulation systems [17–20], electro-magnetic devices connected to electrical shunts [21–35] and piezoelectric patch/stack elements connected to electrical shunts [36–50]. The stiffness and inertia of these devices can be controlled electrically. In this way, the fundamental resonance frequency of the vibration absorber can be suitably varied to either track the frequency of the tonal excitation acting on a hosting system or to follow the resonance frequency that characterises the resonant response of a time-varying hosting structure subject to a broadband stochastic excitation. The damping effect of these devices can be varied electrically too, such that the vibration energy absorption for the tonal and broadband excitations can be properly optimised. Normally, to control tonal vibrations, the natural frequency of the ATVA should closely match the excitation frequency and its damping should be set to rather low values such that, at the excitation frequency, the absorber offers a very high reactive impedance to the hosting system [1–4,51]. Instead, to control broadband resonant vibrations, the natural frequency of the ATVA should be closely tuned to the target resonance frequency and the damping should be set to a critical value such that the absorber maximises the vibration energy absorption from the target resonant response of the hosting structure [51–58].

This paper builds up on Ref. [59] and proposes a novel in-vacuo adaptive beam element, which is composed by a beam-like composite structure encompassing core structured fabrics wrapped in a deflated plastic skin. The middle section of this beam is fixed to a post, which serves as a deflating junction too. The flexural vibration of the resulting two-arm beam is thus characterised by a flapping fundamental mode [60–64], whose dynamics resembles that of a mass-spring-damper classical vibration absorber [1–4]. The fabrics encompass an interwoven construction of truss-like hollowed particles, made using additive manufacturing technology [65]. They are coated in a sealed plastic bag whose interior vacuum pressure is controlled with a miniature pump connected to the post vacuum-junction. The bending stiffness property of this beam-like in-vacuo adaptive beam element can then be modulated by varying the vacuum pressure in the airtight bag. Hence, the fundamental natural frequency of the resulting vacuum-controlled ATVA can be varied online in such a way as to track the frequency of a tonal excitation or to trail changes in the resonant response of a hosting structure. Moreover, it can also be compensated in case of changes in the dynamic response of the in-vacuo beam element itself due to operation (e.g. vacuum leaks) or exogenous effects (e.g. temperature).

Unlike traditional knitted/woven fabrics made from continuous materials, such as for example fibres or wires [66–68], the structured fabrics used here are composed of a framework of interlocked discrete particles that repeat themselves in space in such a way as to form a conforming mesh. They are quite similar to medieval chain armours made by linkages of metal rings [69,70]. These structures exhibit a rather loose bending stiffness at ambient pressure. However, recently, Wang *et al.* [71] have proposed a new layout composed by 3-dimensional truss-like hollowed particles interlocked into a layered chain mail, which is wrapped in a sealed envelope. They have shown that, the bending stiffness of this assembly can be suitably varied by changing the vacuum level in the bag. Indeed, at ambient pressure the chain mail is loose and conforms to the encasing bag; however, the vacuum uniform pressure exerted by the coating envelope forces the particles to interlock and the chain mail to jam such that the whole structure formed by the inner structured fabric stripes and outer plastic envelope becomes rigid [72–80]. The work reported in Ref. [71] has shown that, with a small vacuum level in the casing bag, this composite structure may become more than 20 times stiffer than in its free configuration. This is due to the fact that, unlike materials made of loose solid grains (e.g. granular materials), these fabrics are characterised by interlocked truss-like hollowed grains such that contacts between convex surfaces and between non-convex surfaces may develop amid neighbouring particles (for simplicity, hereafter the two types of contacts will be referred to as “convex contacts” and “non-convex contacts”). As for solid granular materials [81], the convex contacts provide high normal-compressive and tangential-friction resistance [82–85]. Instead, the non-convex contacts, besides the tangential-friction resistance, provide a significant normal-tensile resistance too (e.g. see graph 3 in Ref. [71]), which is instrumental in having a high bending stiffness of the whole in-vacuo beam-like structure considered in this study [71,86,87].

This paper has three objectives. Firstly, to present in a consistent framework the fundamentals of jamming and interlocking of hollowed truss-like chain mail fabrics wrapped in deflated bags and to characterise the dynamic (vibration) response of the beam-like in-vacuo structure considered in this study. Secondly to describe the physics and working principles of the proposed in-vacuo adaptive beam element and to provide a comprehensive analysis of its vibration response. Thirdly to demonstrate that the beam-element can be effectively employed as a vacuum-controlled ATVA for the control of the resonant response of a target vibration mode of a hosting structure. For this purpose, the paper is structured in three main parts organised in Sections 2, 3, 4. To start with, Section 2 is focussed on the physics of in-vacuo chain mail fabrics. More specifically, Section 2.1 presents a comprehensive introduction to the phenomenon of jamming and locking of granular materials, which is then used in Section 2.2 to describe in detail the physics that governs the elastic response of the chain mail fabrics encased in a deflated bag considered in this paper. Then, Sections 2.2 and 2.3 bring together the physics of jamming and locking to explain the mechanical properties of the proposed in-vacuo composite structure; in particular the resistance to bending, which, surprisingly, is particularly high, and the energy dissipation, which, unexpectedly, is limited. Then Section 3 introduces the vacuum-controlled ATVA application. In details, Section 3.2 presents a short, but comprehensive, propaedeutic analysis of the physics of tuneable vibration absorbers set to control the resonant response of a hosting system with a simple and easy to interpret graph comparing the vibration transmissibility and base impedance frequency response functions (FRFs). These FRFs

are then used in Section 3.3 to interpret the experimental measurements taken on a prototype ATVA made with the in-vacuo beam element. Finally, Section 4 presents experimental results on the vibration control effects produced by the proposed vacuum-controlled ATVA on a cantilever beam rig, when the device is tuned to control the resonant response of the fundamental flexural mode.

2. In-vacuo structured fabrics: Working principles, design, fabrication and vibration response

To start with, the jamming and locking phenomena in granular materials is briefly revised here to provide a solid background on the physics that governs the flexural response of the in-vacuo adaptive beam element used to build the vacuum-controlled ATVA. The design and fabrication of the chain mails, as well as their packaging into the airtight bags, are then described in detail. Finally, the vibration responses of the resulting in-vacuo composite beams are analysed with respect to the vacuum level in their bags. This analysis is focussed on two aspects. Firstly, the physics of the flexural response at low frequencies, which has proven equivalent to that of a classical beam made of a homogeneous material. Secondly, the ranges covered by the fundamental flexural resonance frequency and by the damping ratio with respect to the vacuum level, which are relevant for the implementation of adaptive systems, such as, indeed, the ATVA application considered here. The in-vacuo element proposed in this paper is meant for semi-active applications, where its fundamental resonance frequency effect is continuously adapted in such a way as to compensate for changes in the dynamics of both the hosting structure and in-vacuo element itself. Thus, it is not meant to provide an accurate correlation between the imposed vacuum level and the fundamental resonance frequency, but rather to provide the maximum possible tuning range of the resonance frequency.

2.1. Jamming and locking of granular materials

As described in Refs. [79,80], jamming is at the core of rigidity of disordered, amorphous granular materials whose particles interact solely via contact forces. Dry, cohesionless, granular materials can exist only in presence of imposed external loads, such as for example, gravity body forces or external packing forces, i.e. isotropic compression forces. It is a collective phenomenon, where small local variations of the granular layout and particles connectivity alter the mechanical properties of the whole material. Jamming does not conform to ordinary phase transitions based on temperature variations (e.g. phase transitions of metals, glasses, etc.); on the contrary it relies on geometric constraints, that is, contacts between neighbouring particles. Thus, it occurs with a-thermal compounds, which are made by large enough particles such that there is no thermal motion (the energy from thermal fluctuations is much too small to dislocate the grains). Indeed, the jamming transition does not depend on temperature; on the contrary, it is resolved by two parameters, that is: the available free volume per particle, also called packing fraction ϕ, and the shear stress τ applied on the material.

In general, jamming develops when the layout of contacts between neighbouring grains prevents motion of all grains and the applied stress is too small to collapse the grain aggregate. The unjamming transition, that is the rapid loss of rigidity by the whole material, occurs when the particles-filling drops below a critical threshold such that the particles gain mobility and the whole structure becomes compliant. Alternatively, it can also arise when the shear stress exceeds a limit that forces the compound to dilate and yield. Overall, the jamming/unjamming transitions solely depend on the extent to which the grains of the compound block each other. In a jammed state, the forces and moments acting on the aggregate should satisfy static equilibrium conditions on each grain, except for the so-called rattler grains, which do not meet the force or moment equilibrium conditions and thus are free to shake in a limited region of the particles unregular lattice. In case of friction grains, Coulomb equilibrium condition should also be satisfied; that is, the transverse forces acting at the contacts between neighbouring grains should be lower than the friction limit too. In general, the material maintains the disordered/amorphous layout on both unjammed, fluid-like, and jammed, solid-like, phases. In particular, in the jammed rigid phase, it does not develop regular structures, such as crystals.

In contrast to thermal fluid–solid transitions (e.g. metals and alloys), yet there is no firm and comprehensive theoretical framework for the jamming transition of granular compounds. Nevertheless, a unified "phase diagram" was proposed by Liu and Nagel in 1998 [72] for aggregates that form disordered, i.e. amorphous, solids such as foams, colloids, granular materials, glassy molecular systems, etc. and was investigated in detail for compounds of frictionless particles [77]. As shown in Fig. 1a, the Liu-Nagel phase diagram

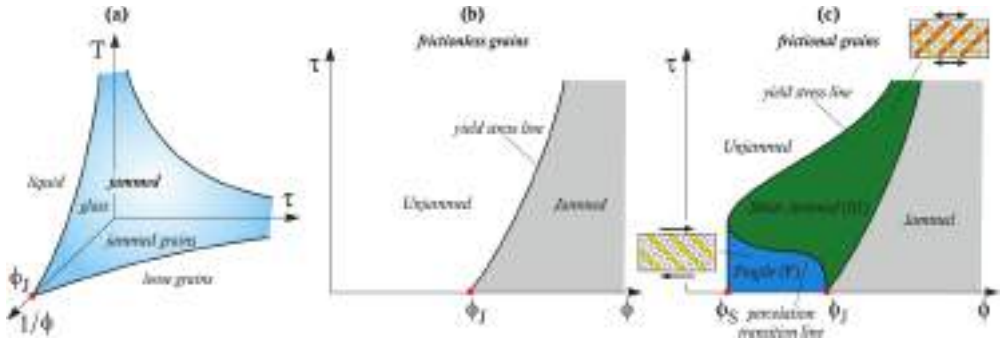

Fig. 1. a) unified phase transition diagram proposed by liu and nagel [72] for amorphous systems, b) jamming phase diagram for frictionless granular aggregates, c) shear jamming phase diagram for frictional granular aggregates (reconstructed from Ref. [79]). Here ϕ is the packing fraction, τ is the shear stress, T is the temperature.

expanded the traditional phase plane for the space density (or packing fraction ϕ) versus temperature (T) by adding the shear stress (τ) dimension. This diagram was first proposed with the intention of unifying the glass transition ($T-\phi$ plane) with the purely athermal jamming transition ($\phi-\tau$ plane). The diagram indicates that there is a lower packing fraction ϕ_J for which isotropic (i.e. shear free) jamming can exist [80], which is normally recalled as the Random Close Packing (RCP) [79].

To investigate the jamming transition, normally the a-thermal plane $\phi-\tau$ shown in Fig. 1b,c is considered. The nature of the contacts, that is of the forces, that develop between neighbouring particles of the aggregate is a key factor for the jamming/unjamming phase transition. For example, if the particles in the aggregate were frictionless [88–91], then only normal forces would develop at contact points between neighbouring particles. Assuming the thermal energies were negligible, and the grains were stiff enough such that they cannot be distorted by the stress applied to the whole aggregate, the jamming transition solely depends on the number and orientation of contacts. For instance, as shown in Fig. 1b, assuming the bulk of grains is not exposed to a shear stress, i.e. $\tau = 0$, then, as the packing increases, and thus the free volume between particles is reduced, the number of contacts between neighbouring grains rises and thus the mobility of the particles progressively falls until it reaches mechanical equilibrium at a critical packing fraction ϕ_J where the material displays both non-zero bulk modulus B and non-zero shear modulus G of elasticity. The transition from the amorphous fluid-like unjammed phase to the amorphous solid-like jammed phase is quite abrupt and, for aggregates made of frictionless spheres, it occurs at the critical value of $\phi_J = 0.64$ [77–81]. The J-point represents a critical phase transition where, likewise molecular fluids nucleate into crystalline-solid, a particle aggregate develops into an amorphous solid. If the packing, that is the free volume, of the particles aggregate was further increased, then the material would withstand larger shear stresses before reaching the jamming/unjamming, i.e. solid/fluid, phase transition. Conversely, if the material was exposed to a shear stress, then jamming will occur to slightly higher critical packing fractions $\phi > \phi_J$, which are defined by the "yield stress line" shown in Fig. 1b. This line divides the a-thermal plane $\phi-\tau$ in two parts, where on the left-hand side the material is in an unjammed state characterised by an amorphous aggregate of free particles, that is a fluid-like material, and on the right-hand side the material is in a jammed state characterised by an amorphous aggregate of blocked particles, that is a solid-like material. In summary, aggregates made with frictionless grains jam either at $\tau = 0$ and $\phi = \phi_J$ or along the yield stress line with $\tau \neq 0$. In general, jamming/unjamming of cohesionless granular materials can be generated either by increasing/decreasing the density, i.e. the packing fraction ϕ, of the material through boundary isotropic compression/decompression or by decreasing/increasing the shear stress τ acting on the material through an applied shear load at the boundary.

If the particles displayed friction [78,92–99], then the critical packing density would extend to $\phi_S < \phi_J$, which is normally recalled as the Random Loose Packing (RLP) [79]. According to Cates *et al.* [100], in this case, when the bulk of grains is exposed to small levels of shear, strong contact forces develop in the material which percolate to the boundary along the compression direction only in such a way as they form parallel filaments-like of forces. As shown by the lower sketch in Fig. 1c, the material forms an anisotropic jamming structure, which can withstand continued shear in this direction but would fall apart if the shear were reversed. This phenomenon leads to the so-called Fragile Jamming (FJ) which, according to Fig. 1c, extends up to the so called "percolation transition line", where, for the given packing fraction ϕ, the imposed stress is large enough to generate strong force networks that percolate to the boundary in all directions such that, as shown by the simplified upper sketch, the material can withstand shear in all directions and thus it can resist to shear reversals too. For aggregates formed by frictionally spheres the RLP packing density is $\phi_S = 0.55$. In general, aggregates made of frictionless particles can be sheared up to packing fractions ϕ_J; instead, in presence of friction, the particles should dilate to shear the aggregate. Therefore, to have shear jamming, the aggregate should be confined in a fixed volume, which leads to the dilation of the particles necessary to develop the shear jamming [80].

The critical density ϕ_J defines a critical point where the amorphous aggregate starts displaying a bulk modulus B and shear modulus G of elasticity. In general, both parameters show a power law scaling with respect to the relative packing density $\Delta\phi = \phi - \phi_J > 0$, where, as $\phi \to \phi_J$ from above, G vanishes continuously whereas B remains constant to then suddenly drop in for values of ϕ close to ϕ_J. Thus, as $\phi \to \phi_J$, there is quite a large ratio B/G, which can be approximated by the following relation $B/G \approx \Delta\phi^{\gamma}$, where $\gamma = 0.5$. This indicates that in the vicinity of point J the granular material is much more susceptible to shear than to isotropic compression and works more like a liquid. Alternatively, as $\phi \gg \phi_J$, the particle aggregate responds more like an ordinary solid both with respect to shear and compression, which may display localised failure zones like brittle materials. The in-vacuo composite structure considered in this study is indeed operated at vacuum levels such that it exhibits a solid-like state having elastic properties, i.e. bulk B and shear G moduli, that span over given ranges to provide the tuning feature necessary to have a vacuum-controlled ATVA.

Beside the confining pressure, that is the volume packing, imposed on a granular material, the elastic properties of the jammed material, i.e. its bulk and shear moduli, B and G, depends on the number and type of contacts between neighbouring particles, which, in turn, depend on the shape, friction coefficient, elastic modulus of the particles themselves. As shown in [101–104], the possibility of fabricating particles with new shapes has emerged with 3D printing, such as Archimedean and Platonic solids, ellipsoids, cuboids, superballs, cylinders, cones, frustums and overlaps of disks and spheres. In this respect, of great interest are particles with non-convex shapes [105–109], such as jacks, dolos, or hollowed particles like the tetrahedral frames. Aggregates with these types of grains are characterised by both convex and non-convex contacts, which lead neighbouring particles to interlock and generate the so-called geometrical friction [110,111] such that new jamming configurations with unique mechanical properties can be generated [71]. Even if the non-convex shapes may lead to lower packing of the aggregate, the interlocked particles are characterised by quite a significant geometrical friction, which can lead to high mechanical properties (e.g. bulk and shear moduli) in front of a much less dense aggregate, that is with a much lighter material. Recent studies have shown that, in presence of a significant network of interlocking contacts, the aggregate would require comparatively much lower confining pressure to generate significant mechanical properties of the jammed material [112,113]. The chain mails employed in this study are indeed formed by complex hollowed truss-like grains such

that, when they are wrapped into a deflated bag, both convex and non-convex contacts are generated by concurrent states of compression and tension due respectively to the jamming and locking effects of the hollowed particles [71], which leads to significant bending stiffness effect.

2.2. Beam-like in-vacuo structured fabric: Design and fabrication

The key component of the proposed in-vacuo adaptive element is the deflated composite beam structure. As shown in Fig. 2, this in-vacuo adaptive beam element is formed by one or multiple core sheets of structured fabrics wrapped by an outer airtight plastic skin (in this study configurations with one or two layers are considered) [59]. The core fabrics are formed by a network of rigid truss-like hollowed elements, which, as depicted in Fig. 3, are interlaced in such a way as to form a loose lattice structure. When the outer plastic bag is deflated, the core fabrics jam and interlock in such a way as they develop both convex contacts and non-convex contacts, where, as discussed above, the latter are characterised by high levels of the so-called geometric friction [110,111]. As can be noticed in Fig. 2, when the chain mail undergoes the isostatic compression exerted by the vacuum bag, to a certain extent, it maintains the lattice structure. Thus, the resulting in-vacuo composite beam does neither show an entirely amorphous layout nor a regular lattice structure. Indeed, it should be classified as a "quasi-amorphous solid" or as a "quasi-crystalline solid" depending on whether one would like to emphasise the jammed underlying layout or the chain-mail primary structure of the material. Nevertheless, the combination of the amorphous and lattice features gives to this material quite unique features, such as low density and fairly high mechanical properties, that is high tensile and compressive resistance, which for the beam-like structure develops into bending resistance too. Rather importantly, the mechanical properties can be suitably modified online by varying the vacuum level in the casing bag, making these materials ideal candidates for the development of innovative smart materials and systems such as, indeed, the in-vacuo adaptive beam element and vacuum-controlled ATVA discussed in this paper.

As shown in Fig. 3, three types of chain mails were fabricated for this study, which have cubic, spherical-octahedral and octahedral hollowed elementary truss-like grains. Table 1 provides the geometries and principal dimension of the three truss-like particles, which occupy a volume of about $0.06cm^3$ each. Also, Table 2 gives the physical properties of the Nylon PA12 material used to fabricate the chain mail fabrics. The structured fabrics built for this study were manufactured by an HP Multi Jet Fusion (MJF) printer. MJF-printed parts can be used both for prototypes and for end-user components. With this technology, additive manufacturing does not need support structures and complex post processing operations. During printing, all empty spaces are filled with wasted powder, making MJF printouts self-supporting. That same powder is then continuously recycled for the following fabrications. MJF can be a successful solution for complex designs: it allows parts consolidation and very complex and interconnected geometries, which is generally a problem using other technologies such as fused deposition modelling (FDM) or stereolithography (SLA).

As shown in Fig. 2, the in-vacuo beam-like composite structures considered in this study were assembled by stacking one or two chain mails in a transparent bag, which had been home-made by bonding along the edges two overlapping plastic films. The dimensions of the plastic sheets were chosen in such a way as to have a rectangular box that would adhere to the loose mesh. A suction pipe was sealed on one side of the bag and was then used to deflate the plastic box in such a way as to modulate the isostatic vacuum pressure exerted on the chain mail and thus its packing volume. As shown by Wang *et al.* (see graph 3 in Ref. [71]), the level of packing infers on the number of convex and non-convex contacts as well as on the nature of the contact forces due to compression-like jamming and tension-like interlocking effects between neighbouring grains. Overall, the result was a beam-like structure displaying a significant flexural resistance effect, where the bending stiffness could be modulated by varying the vacuum level in the bag, that is the packing fraction of the chain mail granular material. In practical applications, it is expected that the beam structure will be made with quite a few layers of overlapping structured fabrics such that it displays comparatively large bending stiffnesses. Moreover, to enhance the bending stiffness, the mails will be entangled on each other with a special three-dimensional knitting fabrication process.

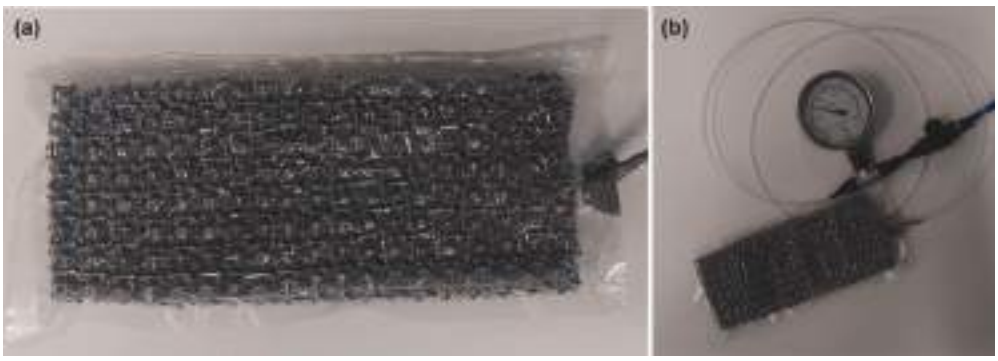

Fig. 2. Beam-like in-vacuo composite structure formed by a core strip structured fabric coated in an airtight plastic bag (a), which is deflated via a small suction pipe (b).

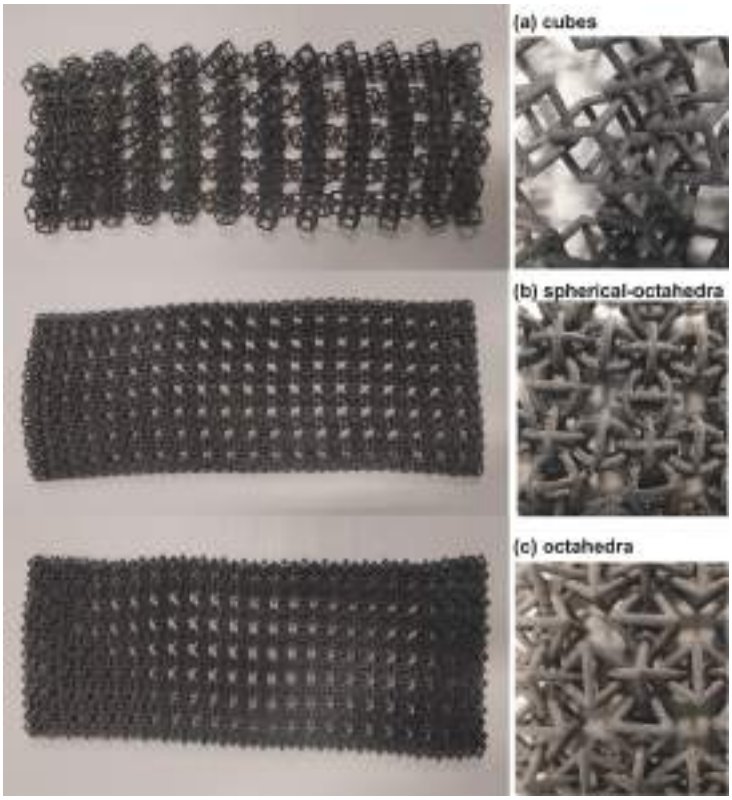

Fig. 3. Structured fabrics encompassing (a) cubic, (b) spherical-octahedral, (c) octahedral truss-like grains.

Table 1
Hollowed truss-like particles used to fabricate the chain mail fabrics employed in this study.

Grains type	Geometry	Width (mm)	Length (mm)	Thickness (mm)	Mass (g)
Cubic		110	190	15	39
Spherical octahedral		100	210	10	49
Octahedral		110	240	15	62

2.3. Beam-like in-vacuo structured fabric: Flexural vibration response

As anticipated above, the proposed in-vacuo adaptive beam element operates in such a way as its bending stiffness can be suitably varied by modulating the vacuum level in the bag encasing the chain mail fabric(s). Hence, its dynamic response is investigated here with respect to the transverse dynamic stiffness FRF measured at the middle section when the beam element is held pinned at the two ends. The results of quite a few tests are presented that were taken on samples encompassing single- or double-layers of the structured fabrics depicted in Fig. 2, which were fabricated with the hollowed truss-like particle listed in Table 2. The transverse dynamic stiffness FRF provides straightforwardly an indication of how the vacuum influences the static and dynamic bending stiffness of the beam-like

Table 2
Nylon PA12 technical specifications.

Property	Value
Powder melting point	187 °C
Particle Size	60 μm
Density of parts	1.01 g/cm^3
Tensile strength	48 MPa
Tensile modulus	1800 MPa
Elongation at break	15–20 %
Bending strength	65–70 MPa
Bending modulus	1730 MPa

elements, that is their fundamental flexural resonance frequency. This is the key parameter for the operation of the proposed in-vacuo adaptive beam element and, indeed, for the vacuum controlled ATVA application investigated in Section 3 below. Assuming time-harmonic vibrations with circular frequency ω, the dynamic stiffness at the centre section of the beam specimen is given by [114]:

$$K(\omega) = \frac{f_b(\omega)}{w_b(\omega)} \tag{1}$$

Here, $w_b(\omega)$ is the complex amplitude of the time-harmonic transverse displacement $w_b(t) = \mathrm{Re}\{w_b(\omega)e^{j\omega t}\}$ imposed at the middle point of the beam span and $f_b(\omega)$ is the complex amplitude of the time-harmonic bending force $f_b(t) = \mathrm{Re}\{f_b(\omega)e^{j\omega t}\}$ resulting at the same point.

The analysis is based on measurements taken with the setup shown in Fig. 4a, which is formed by a base-clamp fixed to a heavy concrete block and a vibrating clamp actuated by a shaker mounted on a stiff steel structure fixed to the same heavy concrete block. As detailed in Fig. 4b, the base-clamp has two posts with sharp jaws, which are used to fix the transverse displacement of the beam ends but leave their rotation free such that, as illustrated in Fig. 4c, they replicate a simply supported boundary condition. Likewise, the vibrating clamp also has sharp jaws such that, as shown in Fig. 4c, a transverse displacement is generated at the middle section of the beam. An impedance head is mounted in between the shaker table and the vibrating clamp to measure the dynamic stiffness FRFs with a two channels spectrum analyser. The FRFs were measured with a two-channels spectrum analyser that implemented a frequency domain analysis based on a random excitation and the derivation of self and cross power spectral density functions from which the FRF between the input and output signals can be suitably calculated (e.g. see examples 9.4 and 9.5 in in Ref. [115]). The analyser provided estimates of the apparent mass FRFs, i.e. complex force over complex acceleration, which were suitably converted into dynamic stiffness FRFs, i.e. complex force over complex displacement, after diving the accelerance by $-\omega^2$.

Moving to the measurement results, Fig. 5 shows the modulus and phase diagrams of the dynamic stiffnesses of the in-vacuo beam-like specimens encompassing either a single (solid-black lines) or two (solid-blue lines) chain mails made with a) cubic, b) spherical-octahedral and c) octahedral particles. The measurements are taken in the low frequency range of interest for the vacuum-controlled ATVA discussed in the forthcoming Sections 3 and 4, which is comprised between 5 and 40 Hz. As specified by the arrows, the diagrams report the measured FRFs for incremental vacuum pressures of 5, 10, 20, 40, 60, 80 kPa. All measurements show similar spectra, with the modulus characterised by a constant value at low frequencies and then a sharp trough, centred at the fundamental resonance frequency, followed by a constant rise proportional to the square of frequency. At low frequencies the phase starts at 0° and then

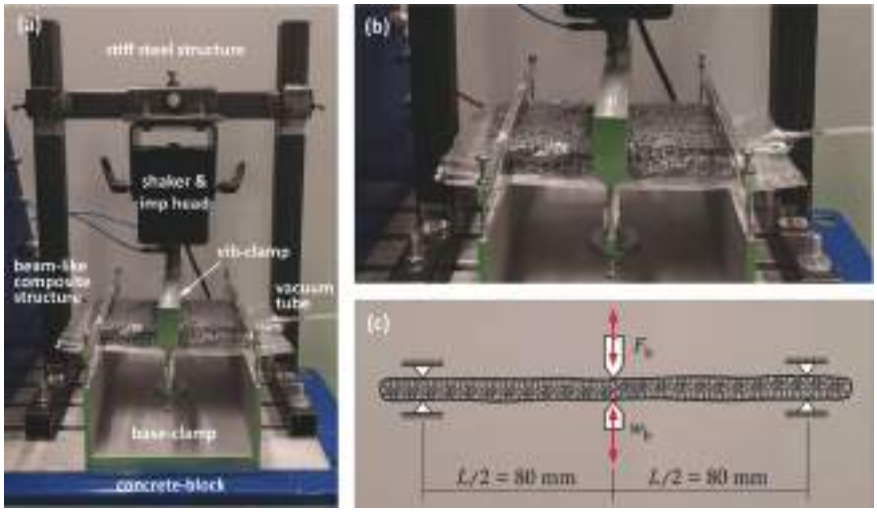

Fig. 4. Six points bending setup for flexural dynamic stiffness measurements.

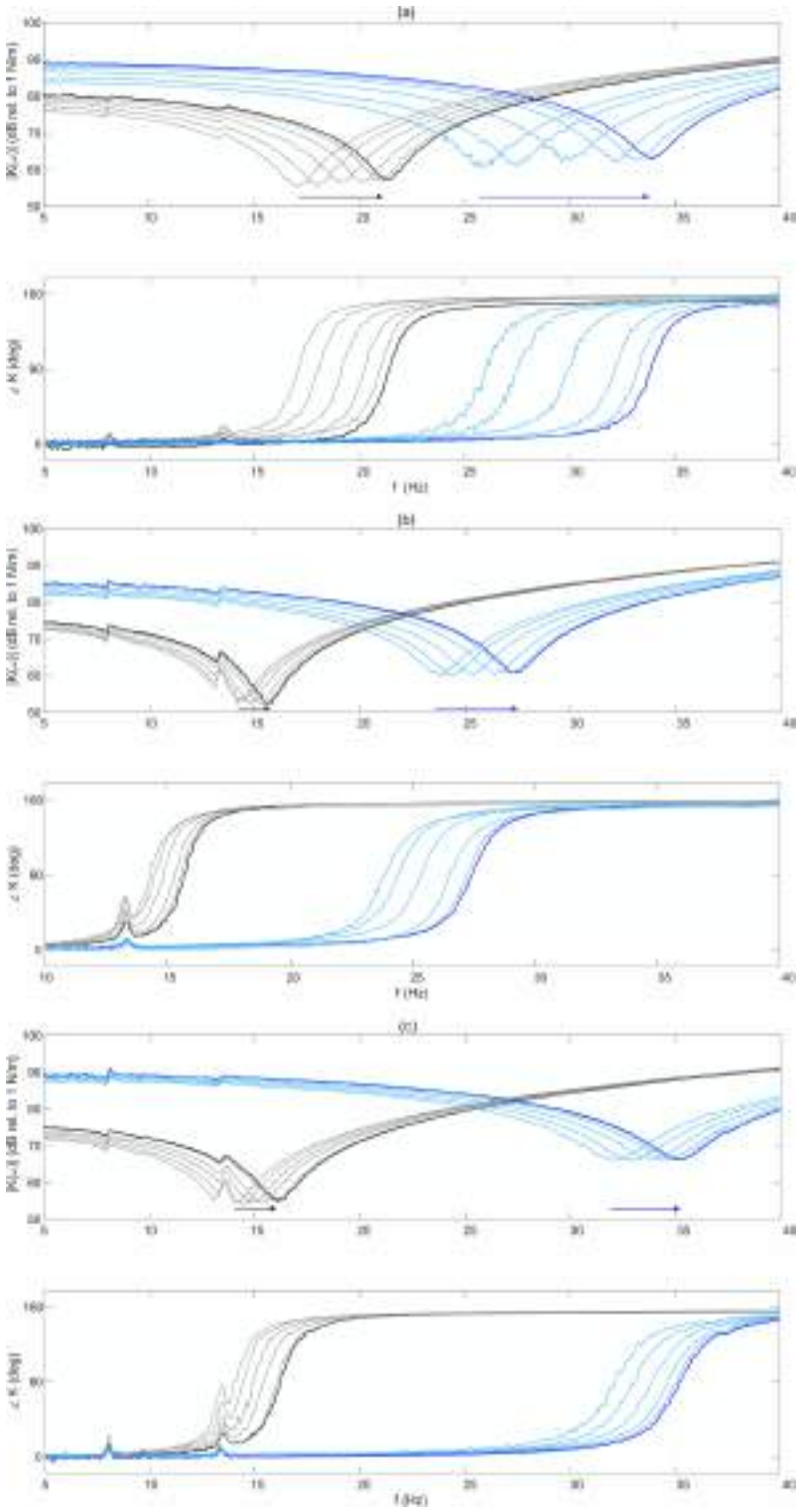

Fig. 5. Dynamic stiffness FRFs of the simply supported beam-like in-vacuo composite structures with core structured fabrics made with cubic (a), spherical octahedral (b) and octahedral (c) particles. Solid-black lines single-layer strips, Solid-blue lines double-layer stripes. Arrows indicate growing vacuum pressures 5, 10, 20, 40, 60, 80 kPa. (For interpretation of the references to colour in this figure legend, the reader is referred to the web version of this article.)

rapidly shifts to $+180^{o}$ in correspondence of the resonance frequency. Hence, overall, the spectra resemble the typical dynamic stiffness of a constrained beam structure at low frequencies, where the response is controlled by the resonant response of the fundamental bending mode [116]. In fact, it displays a stiffness-like response below resonance frequency and a mass-like response above resonance, whereas the resonance trough is controlled by damping [114]. Overall, the diagrams show that the low frequency amplitude of the FRFs, which is controlled by the static bending stiffness of the specimens, tends to raise as the vacuum pressure is brought up. Instead, as one would expect for a fixed mass structure, the high frequency amplitude, which is controlled by the transverse inertia effect of the specimens, tends to the same asymptote that grows proportionally to frequency squared for all vacuum pressures. Consequently, the resonance frequency of the samples tends to raise as the vacuum pressure is brought up.

The graphs in Fig. 5 show dynamic stiffness FRFs, that is the ratio of force over displacement: $K(\omega) = f_b(\omega)/w_b(\omega)$. Hence the sharp troughs in the diagrams of the moduli are due to a resonance effect. Indeed, if the dynamic flexibility given by the reciprocal of the dynamic stiffness, i.e. $\alpha(\omega) = 1/K(\omega) = w_b(\omega)/f_b(\omega)$, were plotted instead, the diagrams of the moduli and phases would show mirrored spectra. In particular, the diagrams of the moduli would show sharp resonance peaks. Hence, the width of the troughs in the spectra of Fig. 5 depend on damping, whose value can be derived with the classical half-power bandwidth formula [117], except that in this case the bandwidth is calculated considering a 3 dB, i.e. $\sqrt{2}$, increment of amplitude of the modulus with respect to its lowest value at the resonance frequency. The diagrams in Fig. 5 show comparable troughs having similar bandwidth, which suggests that the damping does not change much as the vacuum pressure is brought up.

As can be deduced straightforwardly from the spectra in Fig. 5 and from the summary plot in Fig. 6a that reports the resonance frequencies obtained from the peaks in the spectra in Fig. 5, in general, the in-vacuo composite beams encompassing one chain mail display smaller fundamental resonance frequencies f_r than the beams with two overlapped chain mails. For instance, when the vacuum pressure is brought up from 5 kPa to 80 kPa, the resonance frequencies of the beams with a single chain mail made with cubic, spherical octahedra and octahedra span over the following bands 17 – 21.5 Hz, 14.1 – 15.8 Hz, 14 – 16.2 Hz. Hence, when the vacuum is brought up from 5 kPa to 80 kPa, the resonance frequencies raise by 26.4 %, 12 %, 15 % respectively. Alternatively, the resonance frequencies of the beams with a double chain mail made with cubic, spherical octahedra and octahedra cover the following bands 25 – 34 Hz, 23 – 28 Hz, 32 – 35 Hz. Thus, for a 5 kPa to 80 kPa increment of the vacuum in the encasing bags, the resonance frequencies raise by 36.0 %, 21.7 %, 9.3 % respectively. In summary, when the vacuum in the deflated bags is raised from 5 to 80 kPa, the specimens encompassing cubic chain mails show the highest-values and wider-range resonance frequencies. In general, for the 5 to 80 kPa increment of vacuum in the encasing bags, the resonance frequencies of the specimens with two overlapped chain mails are about 60 % to 130 % higher than those of the specimens with one chain Moreover, they span over 30 % wider frequency ranges.

These results confirm that the bending stiffness, and thus the resonance frequency of the fundamental flexural mode, of the in-vacuo composite beams can be suitably modulated by varying the vacuum level in the encasing bags. Indeed, the isostatic vacuum pressure produced on the chain mails by the deflated bag increases the number of contacts between the hollowed truss-like particles and enhances the friction effects such that the composite material displaces higher bulk and shear moduli of elasticity. This is reflected into higher bending stiffness of the samples and thus higher fundamental resonance frequencies. Although this is not a classical homogeneous solid material, the bending stiffness is defined by the geometry of the transverse section of the beam specimen too. In particular, it is linked to the area moment of inertia, which for a rectangular cross section is given by $I_b = bh^3/12$, where b and h are the width and height of the section respectively. Hence, as seen in the measurements, having multiple chain mails shifts to higher values the bending stiffness, and thus the fundamental resonance frequency, of the samples. In this study the arrangement with two structured fabrics was assembled by simply encasing in the plastic bag the two chain mails overlayed one on top of the other such that, during bending, they got jammed but not interlocked. It is thus expected that the stiffness can be raised further with three dimensional mails such that the locking effect would develop both along the length and along the cross section of the beam. The experimental results highlight that the bending stiffness, and thus the fundamental resonance frequency, of the beam specimens depends significantly on the geometry of the hollowed truss-like particles too. For instance, the specimens encompassing two chain mails made with octahedral particles display the highest bending stiffnesses and thus the highest fundamental resonance frequencies, which are comprised be-

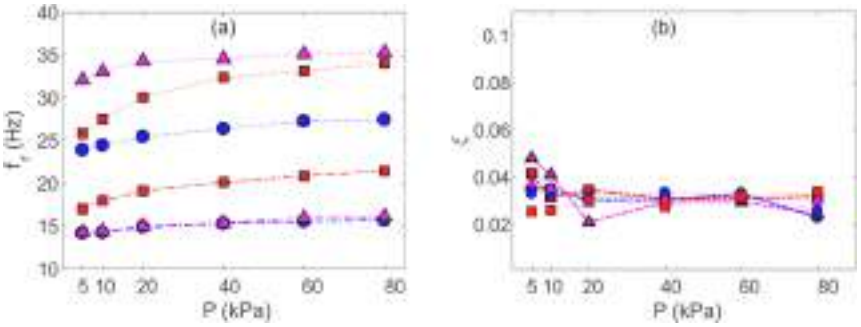

Fig. 6. (a) Resonance frequencies f_r and (b) damping ratio ξ vs. vacuum pressure P of the simply supported beam-like in-vacuo composite structures with one (dash-dotted lines) and two (dotted lines) core structured fabrics. Red lines-squares for cubes, blue lines-circles for spherical octahedra, magenta lines-triangles for octahedra, (For interpretation of the references to colour in this figure legend, the reader is referred to the web version of this article.)

tween 32 and 35 Hz. Nevertheless, the specimen made with two chain mails of cubic particles shows the largest span of bending stiffnesses and thus of fundamental resonance frequencies that encompass a range of 9 Hz comprised between 25 and 34 Hz.

The results presented in this study cover a very limited number of designs of the in-vacuo composite materials. Nevertheless, they have shown how the vacuum pressure, the number of the chain mails, the geometry of the grains infers on the mechanical properties of the beam structures. It is expected that the size of the grains, as well as the material they are fabricated from, should have a significant impact on the jamming and locking phenomena too, both with respect to the number of contacts and in terms of the friction produced at the contact points. Overall, it is foreseen that structures characterised by fundamental resonance frequencies that cover much higher frequencies and span over much wider frequency ranges can be developed by properly choosing a) the type, material and size of the grains, b) the dimensions of the chain mails and c) the number and type of overlayed mails (free to slide or 3D woven).

To complete this analysis, the plot in Fig. 6b summarises the damping ratios that characterise the resonant response of the fundamental bending mode of the beam samples considered in this study. As anticipated above, they were derived from the width of the resonance throughs using the classical half-power bandwidth method [117], which states that the damping ratio is given by the following relation $\xi = 0.5(\omega_2 - \omega_1)/\omega_r$, where, in this case, ω_r is the resonance circular frequency and ω_1, ω_2 are the circular frequencies where the amplitude of the resonance trough is raised by a factor $\sqrt{2}$ with respect to the resonance frequency. The FRFs were measured with a fairly high sampling rate of 0.1 Hz and thus it is expected the damping ratios were estimated quite accurately. This plot presents an entanglement of data in a range of damping ratios comprised between 0.02 and 0.05. On average, the specimens with a double layer of structured fabrics have slightly higher damping than those with a single layer. Overall, these results indicate three important outcomes. Firstly, the level of damping is pretty low for all specimens. Secondly, the vacuum level in the encasing bags does not have a significant effect on damping. Thirdly, the type of particles forming the chain mails has little effect on damping too. These are quite important results, which suggest that the proposed composite material can be swiftly used to tune the bending stiffness, and thus the natural frequency, of the beam specimen without inferring on its damping.

The results presented in this section suggest that the in-vacuo beam element can be suitably used as an adaptive element for vibration control applications. For instance, as will be shown in the forthcoming sections, it can be used as an adaptive tuneable vibration absorber. Indeed, the beam element can be mounted on a post such that it works as a flapping beam whose dynamics resemble that of a mass-spring-damper system, that is of a tuneable vibration absorber. The operational frequency of the device can be swiftly varied over a given range by adjusting the vacuum level in the bag. The nominal centre frequency of operation will depend on the dimension of the beam element as well as the type, geometry and number of chain mails. The tuning range will instead depend on vacuum exerted on the bag.

3. Vacuum-controlled ATVA: design, fabrication, working principles and vibration response

The design and working principles of the vacuum-controlled ATVA application considered in this paper are now analysed in detail. To start with, the actual layout of the absorber is presented, which is made by fixing the in-vacuo adaptive beam element discussed

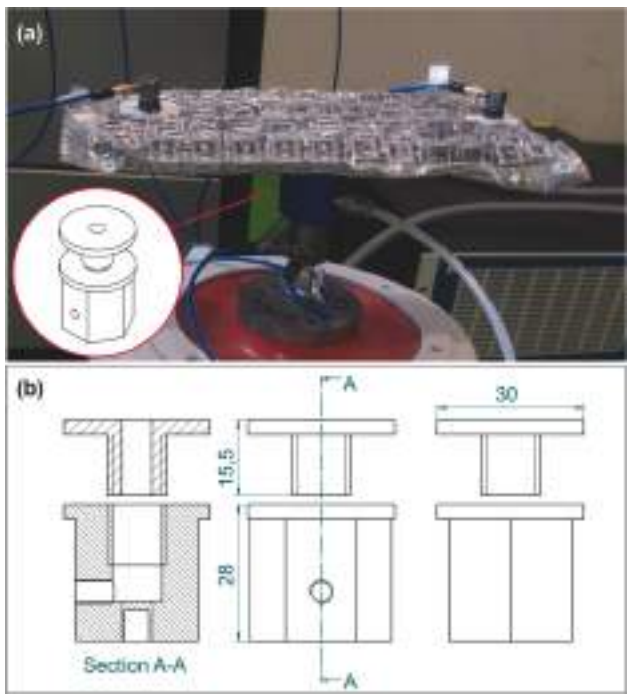

Fig. 7. Vacuum-controlled ATVA mounted on a shaker table (dimension in mm).

above on a post junction. Next, its dynamic response is briefly examined on a qualitative level with simulations assuming it is mounted on a flexible beam structure to control the resonant response of the fundamental flexural mode. Then, the actual dynamic responses of vibration absorber prototypes encompassing the in-vacuo composite beams made with either a single or a double chain mail fabricated respectively with cubic, spherical-octahedral and octahedral grains are thoroughly investigated experimentally. More specifically, to start with, measurements of the displacement transmissibility FRFs between the base junction and two ends of the in-vacuo composite beam are analysed to provide an indication of the flapping response of the beam itself, which is at the basis of the vibration absorption mechanism. Then, measurements of the base impedance FRFs taken at the base post are examined, which provide an indication on its applicability to control the resonant response of a hosting mechanical system or structure.

3.1. Vacuum-controlled ATVA design and fabrication

As anticipated in the Introduction, the in-vacuo composite beam described in the previous Section 2.1 can be used as a tuneable vibration absorber device. To this end, a circular hole has been made in the middle of the bottom sheet of the plastic bag encasing the structured fabric. A specially dedicated post has then been sealed on the hole. As can be noticed in Fig. 7a, the post is a small blue hexagonal component, which has been designed and built with 3D printing technology in such a way as it performs two tasks. Firstly, it acts as a base junction such that the ATVA can be conveniently bolted on a mechanical system or distributed structure via the threaded hole made on the bottom face of the cylindrical element (see Fig. 7b). Secondly, it also works as a plug-in junction for the air suction supply. To this end, as shown in the drawings of Fig. 7b, an L-shaped cavity with circular section was devised inside the junction element, with one termination on its top face where the bottom sheet of the plastic bag is sealed and the other termination on the lateral face where a tube connector is fixed. More specifically, the top opening was threaded in such a way as to screw in a ring stopper that seals the hollowed bottom layer of the bag to the junction. To avoid leakages, butyl sealing tape was used in the thread. The lateral opening of the L-shaped circular cavity was also threaded in such a way as to fix an off-the-shelf connector where to plug in the air suction tube. As can be seen in Fig. 7, a small diameter flexible tube was thus tightened between the junction post and the vacuum rig used to deflate and control the vacuum level in the sealed bag, which was composed of a vacuum pump, a vacuo-meter and a check valve.

3.2. Vacuum-controlled ATVA working principle

Before entering into the details of the dynamic response of the prototype vacuum-controlled ATVA investigated in this study, the tuning and vibration control performance of an ATVA connected to a flexible structure is briefly revised here on a qualitative level in such a way as to highlight upfront what type of mechanical action the absorber should exert on the hosting system to reduce its resonant response. As shown in Fig. 8a, the analysis is inspired to the practical case examined in the forthcoming Section 4 where the in-vacuo adaptive beam element described above is mounted at the tip of a clamped beam to control the resonant response of its fundamental flexural mode. Here, the low frequency response of the hosting beam structure is analysed considering the contribution of the fundamental flexural natural mode only, which is modelled with the modal mass-spring-damper lumped parameter model depicted in Fig. 8b. As discussed in Refs. [60–63] for beam-like vibration absorbers, the low frequency vibration of the two-arms in-vacuo composite beam should be characterised by a flapping bending mode. Hence, as shown in Fig. 8c, the low frequency flexural response of the post and beam assembly can be modelled in terms of a base and seismic mass connected via a spring and damper in parallel. To simplify the analysis, only the response of the fundamental bending mode of the beam is considered with the lumped parameter model depicted in Fig. 8b assuming the physical parameters listed in Table 3, which had been identified with the test rig considered in Section 4.

In this case, the equations of motion for the structural mode and the vibration absorber are given by [4]

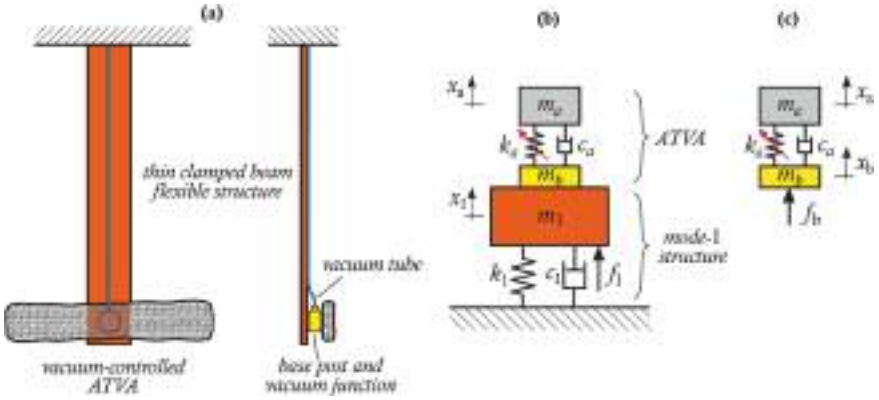

Fig. 8. (a) Beam structure with the proposed vacuum-controlled ATVA for the control of the resonant response of a target flexural mode. (b) Equivalent lumped model for the resonant response of the target mode and vacuum-controlled ATVA. (c) Lumped model of the vacuum-controlled ATVA.

Table 3
Physical parameters of the lumped element system shown in Fig. 8b,c used for the qualitative analysis of the vacuum-controlled ATVA system depicted Fig. 8a, which had been identified from the rig considered in Section 4.

Component	Property	Value
Beam	Natural frequency	$f_1 = 38\text{Hz}(\omega_1 = 238.7 rad/s)$
fundamental natural mode	Damping ratio	$\xi_1 = 0.02$
	Modal mass	$m_1 = 0.340\text{kg}$
	Modal stiffness	$k_1 = (m_1 + m_b)\omega_1^2 = 22120\,\text{N/m}$
	Modal damping	$c_1 = 2m_1\omega_1\xi_1 = 3.6\,\text{N/ms}^{-1}$
Optimal ATVA	Seismic mass	$m_a = 0.052\text{kg}$
(tuning parameters were taken from Tab. 1 of Ref. [58] for the minimisation of the time average kinetic energy of the hosting system).	Base mass	$m_b = 0.024\text{kg}$
	Mass ratio	$\mu = m_a/(m_1 + m_b) = 0.14$
	Optimal frequency ratio	$\nu_{a,opt} = 1/\sqrt{1+\mu} = 0.94$
	Natural frequency	$f_{a,opt} = \nu_{a,opt} f_1 = 35.6\text{Hz}(\omega_1 = 223.3 rad/s)$
	Stiffness	$k_{a,opt} = m_a\omega_a^2 = 2594\,\text{N/m}$
	Optimal damping ratio	$\xi_{a,opt} = \sqrt{\mu}/2 = 0.19$
	Damping	$c_{a,opt} = 2m_a\omega_{a,opt}\xi_{a,opt} = 4.4\,\text{N/ms}^{-1}$

$$(m_1 + m_b)\ddot{x}_1 = -c_1\dot{x}_1 - k_1 x_1 + c_a\left(\dot{x}_a - \dot{x}_1\right) + k_a(x_a - x_1) + f_1 \tag{2}$$

$$m_a\ddot{x}_a = -c_a(\dot{x}_a - \dot{x}_1) - k_a(x_a - x_1) \tag{3}$$

As specified in Fig. 8, m_1, c_1, k_1, f_1 are the modal mass, damping, stiffness and modal force for the first bending mode of the beam structure and m_b, m_a, c_a, k_a are the base mass, seismic mass damping factor and stiffness of the vacuum-controlled ATVA. Assuming the time-harmonic displacements and force excitation are given in the complex form $x_1(t) = \text{Re}\{x_1(\omega)e^{j\omega t}\}$, $x_a(t) = \text{Re}\{x_a(\omega)e^{j\omega t}\}$, $f_1(t) = \text{Re}\{f_0 e^{j\omega t}\}$, where $x_1(\omega)$, $x_a(\omega)$ are the complex amplitudes of the displacements and f_0 is the amplitude of the force excitation, after some mathematical steps, the complex amplitude of the mode-1 displacement for the beam without and with vacuum-controlled

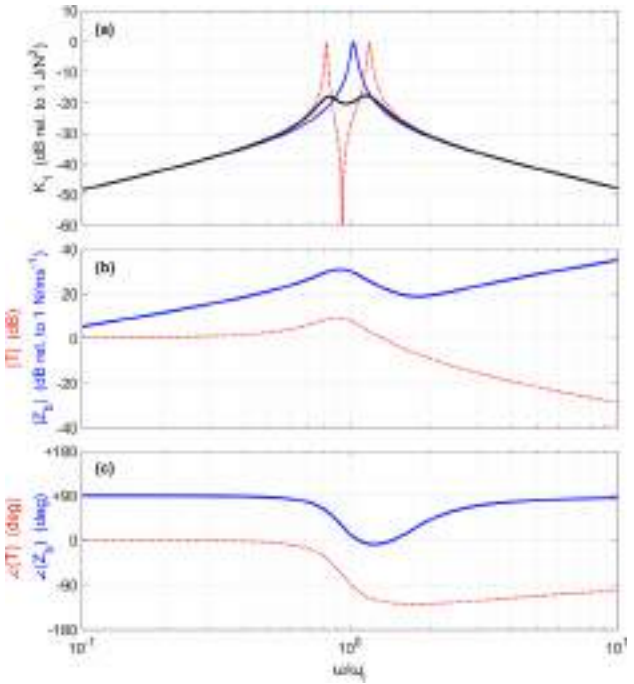

Fig. 9. (a) Spectra of the time-averaged flexural kinetic energy $K_1(\omega)$ of mode 1 of the structure depicted in Fig. 7. Beam without (solid blue line) and with lightly-damped (dotted red line) and optimally-damped (solid black line) ATVA. (b) and (c) spectra of the modulus and phase of the vibration transmissibility $T(\omega)$ (dotted red line) and base impedance $Z_b(\omega)$ (solid blue line) of the optimally tuned ATVA. (For interpretation of the references to colour in this figure legend, the reader is referred to the web version of this article.)

ATVA is given respectively by [4]

$$x_1(\omega) = \frac{1}{k_1 - \omega^2(m_1 + m_b) + j\omega c_1} f_0 \tag{4}$$

$$x_1(\omega) = \frac{(k_a - \omega^2 m_a + j\omega c_a)}{[(k_1 + k_a) - \omega^2(m_1 + m_b) + j\omega(c_1 + c_a)](k_a - \omega^2 m_a + j\omega c_a) - (k_a + j\omega c_a)^2} f_0 \tag{5}$$

To provide a simple analysis consistent with the experimental results presented in Section 4, the response of the beam without ATVA in Eq. (4) has been derived assuming the ATVA base mass remains connected to the hosting beam structure. For the stationary time-harmonic excitation, the response of the fundamental flexural mode of the hosting beam can be derived for each excitation frequency with respect to its time-averaged total flexural kinetic energy, which is given by

$$K_1(\omega) = \frac{1}{T}\int_0^T \frac{1}{2} m_1 \dot{x}_1^2 dt = \frac{1}{4} m_1 \omega^2 |x_1(\omega)|^2 \tag{6}$$

where T is the period of the time-harmonic vibration.

To provide a clear description of the action that the vibration absorber should produce on the hosting system, the graphs of the absorber vibration transmissibility and base impedance have been assembled together in Fig. 9 on a single modulus-phase diagram aligned below the classical diagram with the spectrum of the response of the hosting system without and with the optimally tuned ATVA, as it is normally presented in textbooks [1–4]. More specifically, the solid blue line in Fig. 9a shows the spectrum of the time-averaged kinetic energy $K_1(\omega)$ for the beam without the vacuum-controlled ATVA. The spectrum is characterised by the typical sharp resonance peak at the fundamental resonance frequency, which for the lightly damped structure at hand is close to the natural frequency $\omega_1 = \sqrt{k_1/(m_1 + m_b)}$ of the fundamental flexural mode. The amplitude of this peak can be effectively mitigated by adding to the beam the in-vacuo vibration absorber properly tuned. As summarised in Tab. 1 of Ref. [58], over the years quite a few criteria were proposed to optimally tune a vibration absorber, which have been expressed with respect to two tuning parameters, that is, the damping ratio of the absorber $\xi_a = c_a/(2m_a\omega_a)$ and the frequency ratio $\nu = \omega_a/\omega_1$ taken with respect to the natural frequency of the absorber held blocked at the base, that is $\omega_a = \sqrt{k_a/m_a}$. In this study the criterion based on the minimisation of the time-averaged kinetic energy of the hosting structure exposed to a wide band stationary stochastic excitation is employed, which, considering the mass ratio $\mu = m_a/(m_1 + m_b)$, gives the following optimal parameters: $\xi_{a,\text{opt}} = \sqrt{\mu}/2$ and $\nu_{\text{opt}} = 1/\sqrt{1+\mu}$ [58]. To comply with the beam rig and vacuum-controlled ATVA considered in Section 4, the mass ratio was assumed equal to $\mu = 0.15$. In this case, if the damping ratio of the absorber were kept to a very low value, e.g. $\xi_a = 0.005$, and the stiffness of the absorber were tuned in such a way as its natural frequency complies with the criterion for the ν_{opt}, i.e. $\omega_a = \nu_{\text{opt}}\omega_1$, then the spectrum of the kinetic energy $K_1(\omega)$ of the beam with the vacuum-controlled ATVA would be characterised by a double peak as depicted by the dotted red line in Fig. 9a. Now, if the damping of the vibration absorber were optimally tuned in such a way as that $\xi_a = \xi_{a,\text{opt}}$, then, as depicted by the solid black line in Fig. 9a, the two peaks would be smoothened out such that, overall, the spectrum of the flexural kinetic energy would be significantly lowered at frequencies close to the natural frequency of the target mode of the hosting beam. This indicates that, if for example the beam was excited by a stationary broadband excitation, the resonant response produced by the first natural mode of the beam would be substantially attenuated too.

To complete this introductory analysis, the dynamic response of the vibration absorber and the dynamic load generated by the vibration absorber on the hosting structure are examined by considering respectively the displacement transmissibility FRF between the base and seismic masses and the base impedance FRF of the absorber optimally tuned. Assuming the time-harmonic displacements and base force specified in the lumped parameter model in Fig. 8c are given by $x_b(t) = \text{Re}\{x_b(\omega)e^{j\omega t}\}$, $x_a(t) = \text{Re}\{x_a(\omega)e^{j\omega t}\}$ and $f_b(t) = \text{Re}\{f_b(\omega)e^{j\omega t}\}$, the transmissibility and base impedance FRFs are given by:

$$T(\omega) = \frac{x_a(\omega)}{x_b(\omega)} \tag{7}$$

$$Z_b(\omega) = \frac{f_b(\omega)}{j\omega x_b(\omega)} \tag{8}$$

where $x_b(\omega)$, $x_a(\omega)$, $f_b(\omega)$ are the complex amplitudes of the time-harmonic displacements $x_b(t)$, $x_a(t)$ and force $f_b(t)$. Considering the lumped parameter model of the vibration absorber shown in Fig. 8c, the following two equations of motion can be derived

$$m_b\ddot{x}_b = c_a\left(\dot{x}_a - \dot{x}_b\right) + k_a(x_a - x_b) + f_b \tag{9}$$

$$m_a\ddot{x}_a = -c_a\left(\dot{x}_a - \dot{x}_b\right) - k_a(x_a - x_b) \tag{10}$$

In this case too, after few mathematical steps the displacement transmissibility and the base impedance FRFs are derived as follows:

$$T(\omega) = \frac{(k_a + j\omega c_a)}{(k_a - \omega^2 m_a + j\omega c_a)} \tag{11}$$

$$Z_b(\omega) = \frac{(k_a - \omega^2 m_b + j\omega c_a)(k_a - \omega^2 m_a + j\omega c_a) - (k_a + j\omega c_a)^2}{(k_a - \omega^2 m_a + j\omega c_a)} \tag{12}$$

Fig. 9b and 9c show the modulus and phase of the displacement transmissibility FRF (dotted red lines) and base impedance FRF (solid blue lines) of the optimally tuned ATVA. Considering first the FRF of the displacement transmissibility $T(\omega)$, at low frequencies below the fundamental natural frequency ω_a of the ATVA, the transmissibility is characterised by unit amplitude and phase equal to 0°. Hence the two masses oscillate together as if they were a solid body of mass $m_{TVA} = m_b + m_a$. There is then a distinctive resonance peak with amplitude 10dB and phase −90°, which indicates the oscillation of the seismic mass is in quadrature and about 3 time larger with respect to that of the base mass. In other words, the absorber is characterised by a breathing vibration mode with large strokes of the suspension spring and large stroke-rates of the damper, which are at the basis of the vibration absorption and dissipation mechanisms

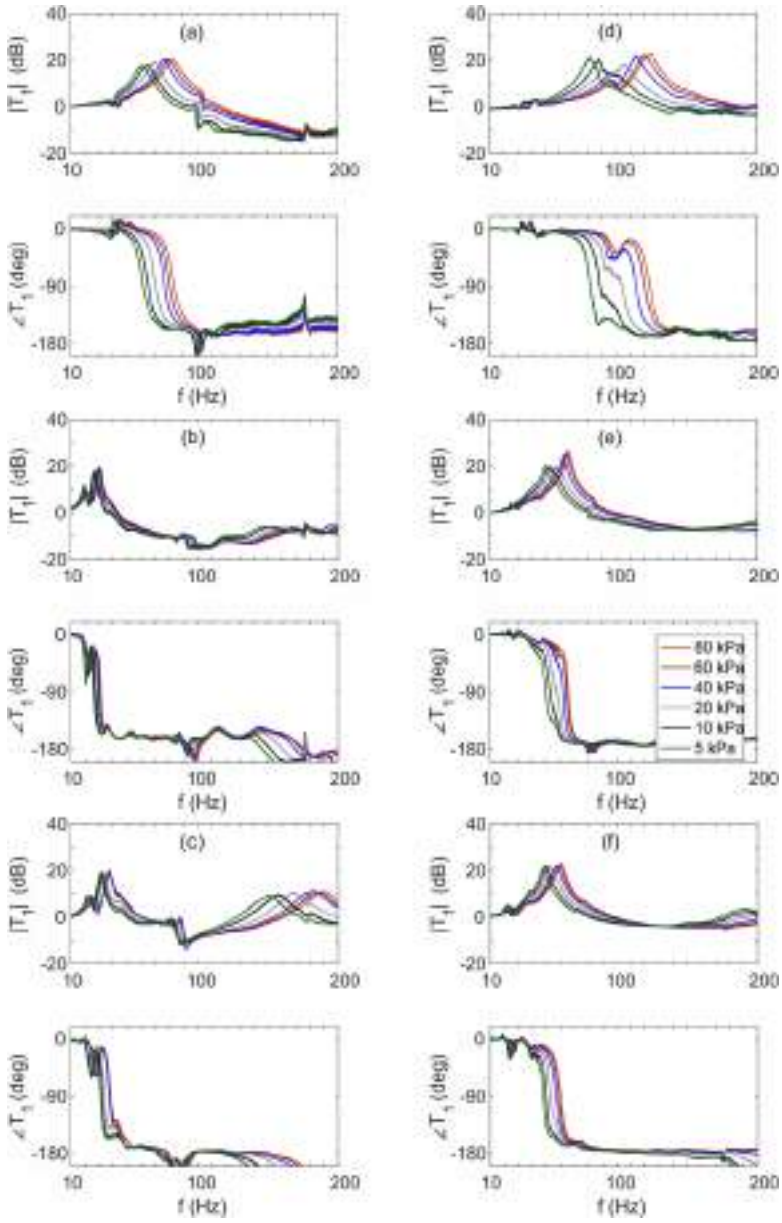

Fig. 10. Transmissibility FRFs $T_1(\omega)$ of the vacuum-controlled ATVA with the composite beam encompassing one (a,b,c) or two (d,e,f) core layers made with cubic (a,d) spherical octahedral (b,e), and octahedral (c,f) particles.

of the ATVA. At higher frequencies above resonance, the transmissibility progressively falls down and becomes smaller than one with phase -180^o, which indicates that, compared to the imposed base displacements, the seismic mass is characterised by progressively smaller, out of phase, displacements. At high frequencies the seismic mass works as an inertial reference block against which the ATVA spring and damper undergo the displacement and velocity imposed at the base.

Moving to the plot of the base impedance function, considering the typical impedance laws of mass, spring and damper elements (e.g. see Fig. 9.2a in Ref. [114]), the two plots indicate that, at low frequencies the base impedance rises proportionally to frequency with phase $+90^o$, and hence it is controlled by the mass effect of the whole ATVA, which, as discussed above, vibrates as a rigid body. At high frequencies it also rises proportionally to frequency with phase $+90^o$, but, in this case, it is controlled by the effect of the ATVA base mass only, since, as seen above, compared to the base mass m_b, the seismic mass m_a is characterized by rather small oscillations. In between these two asymptotic responses, there is a resonance peak at about $\omega_a = \nu_{\text{opt}}\omega_1$ followed by an antiresonance trough. Here, the impedance function falls proportionally to frequency with the phase that tends to -90^o, which indicates a stiffness-controlled response. The amplitude of the resonance peak is controlled by the absorber damping effect, which is set to $c_a = 2m_a\omega_a\xi_{a,\text{opt}}$. This diagram indicates that the optimally tuned absorber generates a very high damping impedance effect at the tuning frequency, that is

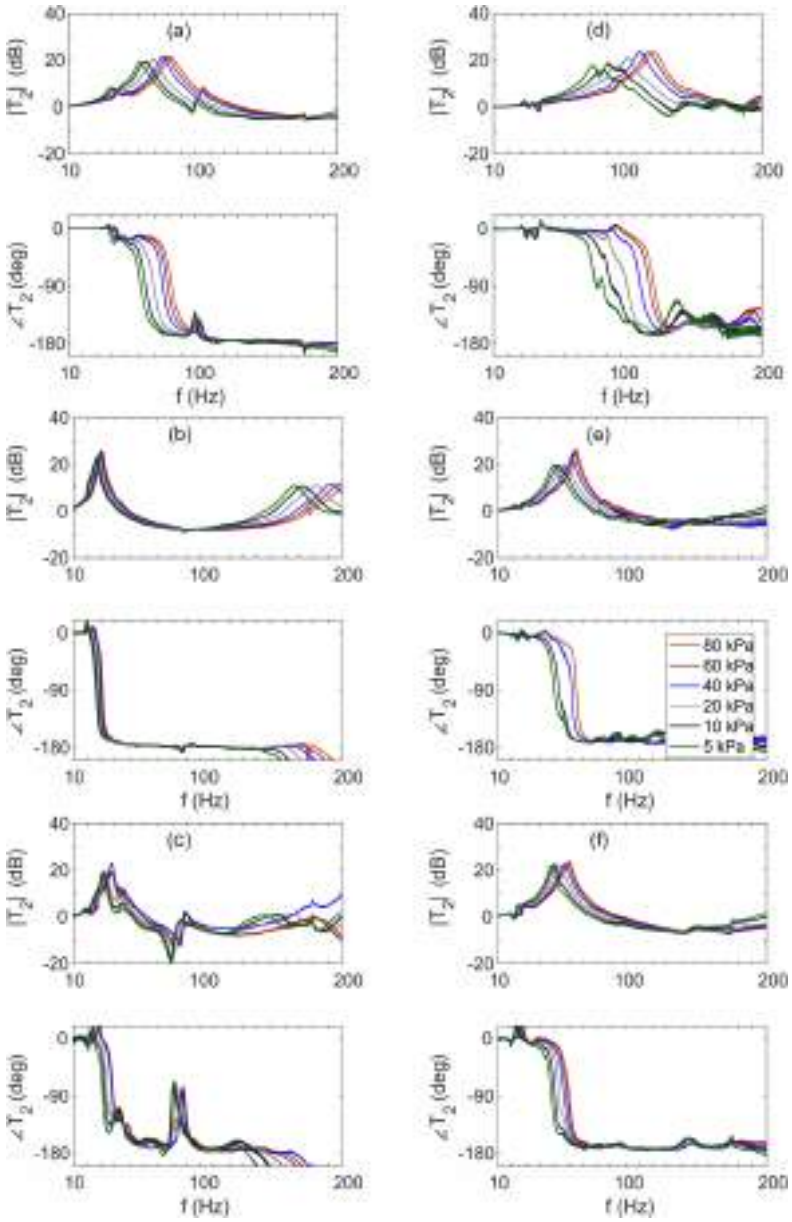

Fig. 11. Transmissibility FRFs $T_1(\omega)$ of the vacuum-controlled ATVA with the composite beam encompassing one (a,b,c) or two (d,e,f) core layers made with cubic (a,d) spherical octahedral (b,e), and octahedral (c,f) particles.

the natural frequency of the hosting system, such that it effectively dissipates the vibration energy of the resonant response of the hosting structure. Overall, the vacuum-controlled ATVA application proposed in this paper, should be designed in such a way as it can generate a vibration transmissibility and a base impedance having spectra like those shown in Fig. 9b,c.

3.3. Vacuum-controlled ATVA vibration response of the in-vacuo adaptive beam element

The design of the vacuum-controlled ATVA presented in the previous section is based on the assumption that the low frequency flexural vibration of the in-vacuo composite beam fixed onto the post is controlled by a flapping fundamental mode, which reproduces the dynamics described above. The validity of this assumption is now assessed with respect to measurements of the displacement transmissibility FRF between the post and the two ends of the beam element forming the vacuum controlled ATVA, which have been taken with the shaker and the base impedance and accelerometers setup shown in Fig. 7. The two transmissibility FRFs were measured for the whole set of ATVAs assembled with the in-vacuo composite beams examined in Section 2.1, which were fabricated either with a single or a double chain mail encompassing the cubic, spherical-octahedral, octahedral truss-like grains whose geometry and physical

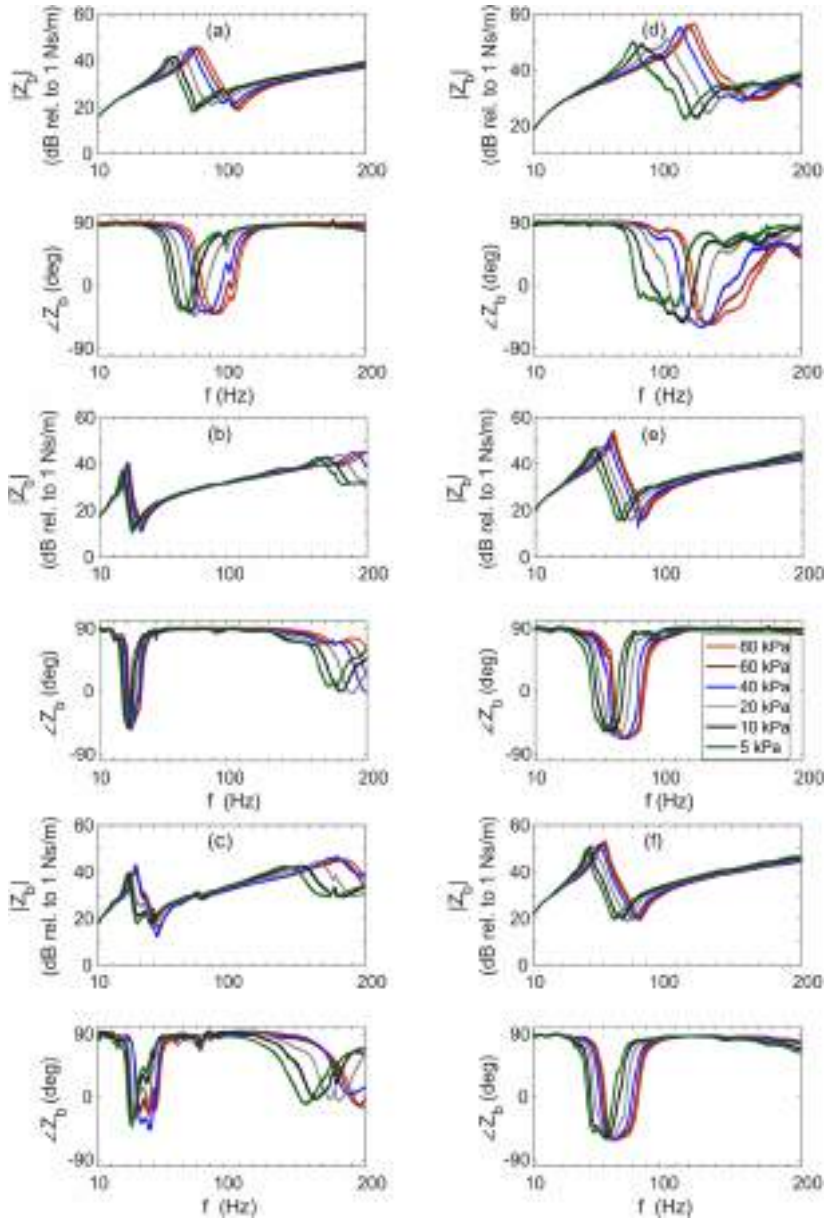

Fig. 12. Base impedance $Z_b(j\omega)$ FRFs of the vacuum-controlled ATVA with the composite beam encompassing one (a,b,c) or two (d,e,f) core layers made with cubic (a,d) spherical octahedral (b,e), and octahedral (c,f) particles.

properties are summarised in Tables 1 and 2. Figs. 10 and 11 show the transmissibility functions $T_1(\omega) = w_1(\omega)/w_b(\omega)$ and $T_2(\omega) = w_2(\omega)/w_b(\omega)$ for the displacement ratios measured between the beam left-hand side termination and the base junction and between the beam right-hand side termination and the base junction in the 10 – 200 Hz range. In general, the graphs agree with the transmissibility FRF shown in Fig. 9. Indeed, the two sets of spectra show that, at low frequencies the transmissibility functions have unitary amplitude (0 dB) and phase equal to 0°, which confirms that the beam vibrates as a solid structure. There is then a resonance peak where the phase shifts to −180°. At higher frequencies the amplitude of the transmissibility falls below 1 (0 dB) and the phase remains at −180°, which indicates the two terminations of the in-vacuo composite beam vibrate much less than the centre post. The spectra contain few more features, which are possibly due to coupled torsional vibrations of the composite beam and also to dynamic effects generated by the rim of the plastic bag. Nevertheless, these artefacts are comparatively much smaller than the principal layout of the spectrum just described. Hence it can be concluded that at low frequencies below 200 Hz, the flexural vibration of the in vacuo composite beam mounted on the post element is characterised by a flapping vibration mode where the left-hand and right-hand side bays of the beam vibrate in phase as if they were two cantilever beams clamped at the base post. In particular, at low frequencies below the fundamental resonance frequency of this mode, the flapping vibration is actually negligible and it can be assumed the in-vacuo composite beam vibrates as a rigid body. Instead, at the resonance frequency there is a fairly large flapping oscillation, which produces an amplitude magnification of 20 dB, that is one order of magnitude. At higher frequencies above the flapping mode resonance frequency, the transmissibility falls down below 1 (0 dB) with phase −180°, which indicates the flapping vibration of the in-vacuo beam is characterised by comparatively larger vibrations of the centre post than the two ends of the beam. Overall, the layout of the vibration transmissibility spectra indicate that flexural response of the proposed vacuum-controlled ATVA can be modelled with the lumped parameter model discussed in Section 3.2 and shown in Fig. 8b,c. Indeed, it can be seen as a seismic mass mounted on a base mass via a spring and damper component, whose vibration can be synthetised as a rigid body vibration up to the fundamental resonance frequency where there is a high counter vibration effect between the base and seismic mass, which produces the vibration absorption and dissipation through the damper. This is followed by a higher frequency response where the seismic mass is characterised by much smaller vibrations than the base mass. In summary, the proposed vacuum-controlled ATVA can be suitably employed as a tuneable vibration absorber whose fundamental natural frequency can indeed be shifted by varying the vacuum level in the deflated bag. To conclude this analysis, it is observed that, the FRFs presented in Fig. 10 and Fig. 11 confirm the findings discussed in Section 2.2 for the dynamic stiffness of the in-vacuo composite beam samples. Indeed, the fundamental resonance frequency of the flapping vibration mode monotonically rises as the vacuum pressure in the deflated bags is brought up. Also, absorbers incorporating the beams fabricated with two overlapped chain mails show comparatively higher fundamental resonance frequency than the absorbers having equivalent beam samples made, however, with a single chain mail. In general, the flapping fundamental resonance frequency is higher for the absorbers made with cubic hollowed truss-like particles and, also, spans over a wider frequency range when the vacuum pressure is raised from 5 to 80 kPa.

3.4. *Vacuum-controlled ATVA vibration absorption with respect to its base impedance*

The analysis of the proposed vacuum-controlled ATVA is concluded here by considering the base impedance FRF, which, as discussed in Section 3.2, gives an indication of the mechanical effects (i.e. mass, stiffness, damping effects) exerted by the absorber on the structure where it is fixed. Fig. 12 shows the modulus and phase of the base impedance FRFs, $Z_b(\omega) = f_b(\omega)/\dot{w}_b(\omega)$, measured on the ATVA encompassing either a single (left hand side plots) or a double (right hand side plots) layer of cubic, octahedral spherical and octahedral structured fabrics. As for the dynamic stiffness analyses, each plot shows six spectra obtained for the six confining vacuum pressures reported above. The spectra show the typical base impedance of a seismic mass connected to a base mass via a spring damper lumped element. Indeed, as discussed in Ref. [114] for example, at low frequencies the spectrum is characterised by a modulus that rises proportionally to the circular frequency and a constant phase value of about $+90^{\circ}$. There is then a resonance peak followed by an antiresonance through, with the phase that initially falls down to -90° and then recovers to $+90^{\circ}$. At higher frequencies the spectrum

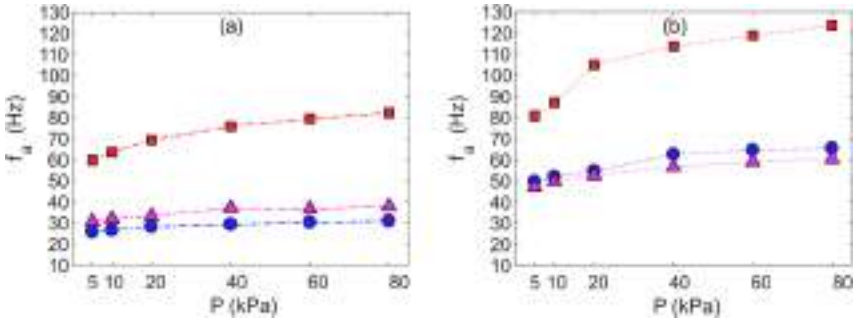

Fig. 13. (a) Resonance frequencies f_a vs. vacuum pressure P of the ATVA made with the in-vacuo beam-like structure with one (dash-dotted lines) (a) or two (dotted lines) (b) core structured fabrics made with cubic (red lines-squares) spherical octahedral (blue lines-circles) and octahedral (magenta lines-triangles) particles. (For interpretation of the references to colour in this figure legend, the reader is referred to the web version of this article.)

shows again a modulus that rises proportionally to the circular frequency and a phase that maintains the $+90^{\circ}$ value. All this indicates that at low and high frequencies the device presents a mass effect. More precisely, the measurements taken with the accelerometers have shown that at low frequencies the in-vacuo structured fabric beam behaves as a solid body together with the junction component, with negligible flapping effects. Therefore, the base impedance is given by the whole mass of the beam and base component. Alternatively, at higher frequencies, despite the base vibrations, the two ends of the in-vacuo structured fabric are characterised by little vibrations such that the base impedance is controlled by the mass of the base component. At resonance frequency, the two ends of the in-vacuo structured fabric display large counter oscillations to the base oscillations, which generate the desired vibration absorption effect. The extent of these oscillations is controlled by the damping of the in-vacuo structured beam.

Overall, the plots shown in Fig. 12 together with the two plots reported in Fig. 13 indicate that the resonance frequency of the vacuum controlled ATVAs can be suitably shifted to higher/lower values by increasing/lowering the vacuum level in the bags. For the 5 to 80 kPa pressure range, the single layer ATVAs are characterised by resonance frequencies comprised between 60–85 Hz (cubic grains), 25–30 Hz (spherical octahedral grains), 30–40 Hz (octahedral grains). Alternatively, the double layer ATVAs are characterised by resonance frequencies comprised between 80–125 Hz (cubic grains), 50–65 Hz (spherical octahedral grains), 45–60 Hz (octahedral grains). This confirms that the resonance frequency of the vacuum-controlled ATVAs can be suitably tuned over significant ranges by varying the vacuum pressure. Moreover, these ranges can be further enlarged by adopting multiple layers with combinations of different grains.

To conclude, the two plots shown in Fig. 14 indicate that the vacuum pressure has little effects on the damping ratio of the ATVA fundamental resonances. Also, the ATVAs assembled with the in-vacuo composite beam with either a single or a double chain mail are characterised by damping ratios confined in the ranges 0.04 – 0.07 and 0.02 – 0.08 respectively. In general, apart from low pressures, the chain mails made with spherical octahedral particles seem to produce slightly lower levels of damping than those made with the octahedral or cubic grains.

4. Vacuum-controlled ATVA mounted on a clamped beam: Experimental results

The actual implementation of the vacuum-controlled ATVA application considered in this paper is now investigated for the case where one of the prototype absorbers analysed in Section 3 is mounted at the free end of a clamped beam in order to control the resonant response of the fundamental flexural mode.

4.1. Test setup

Fig. 15 shows the experimental rig used to test the vacuum-controlled ATVA. As shown in Pictures (a) and (b), the setup is composed by a rigid framework structure with a solid post where a thin beam structure is clamped. The beam is made of steel and has rectangular cross section $b \times h = 30 \times 2$mm. Also, the free length of the cantilever beam is $L = 514$mm. The beam is excited in bending at position $x_f = 40$mm by a transverse force exerted by a shaker via a stinger, which has been equipped with a force cell to measure the force at the excitation point. The flexural response of the beam is measured at the tip of the beam with a small accelerometer. The total mass of the beam inclusive of the force cell and accelerometer is $M_b = 0.340$kg. The beam is equipped with a vacuum-controlled ATVA like that shown in Fig. 7, made with a deflated beam element encompassing a single chain mail composed by spherical octahedral grains. As reported in Table 1, the chain mail weights $M_{cm} = 0.049$kg and the total weight of the in-vacuo beam element is $M_{cm} = 0.052$kg, that is about 14 % of the weight of the cantilever beam. To ensure the total weight of the ATVA does not infer significantly on the response of the beam, the in-vacuo beam element of the ATVA was fixed directly onto the beam without the base junction. More precisely, the centre section of the element was glued close to the free-end of the beam, that is at $x_c = 349$mm.

The dynamic effect produced by the vacuum-controlled ATVA on the clamped beam has been assessed with respect to the spectrum of the transverse velocity at the tip of the beam per unit force excitation exerted by the shaker. Two measurements were implemented in the frequency range comprised between 15 and 60 Hz, where the flexural response is controlled by the fundamental flexural mode of the beam setup. To start with the flexural response of the beam was measured without the vacuum-controlled ATVA. Then the response was assessed with the vacuum-controlled ATVA tuned in such a way as to control the resonant response of the fundamental mode of the beam. The absorber discussed here has been conceived in such a way as it can be continuously adapted to control the resonant response of a target mode of the hosting structure by varying online the vacuum level in the deflated bag, which, as seen above, infers on the

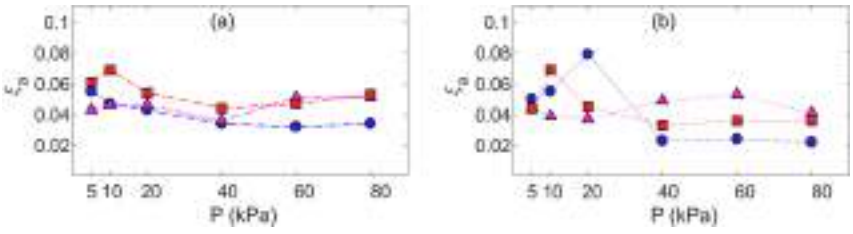

Fig. 14. (a) Damping ratios ξ_a vs. vacuum pressure P of the ATVA made with the the in-vacuo beam-like structure with one (dash-dotted lines) (a) or two (dotted lines) (b) core structured fabrics made with cubic (red-lines squares) spherical octahedral (blue lines-circles) and octahedral (magenta lines-triangles) particles. (For interpretation of the references to colour in this figure legend, the reader is referred to the web version of this article.)

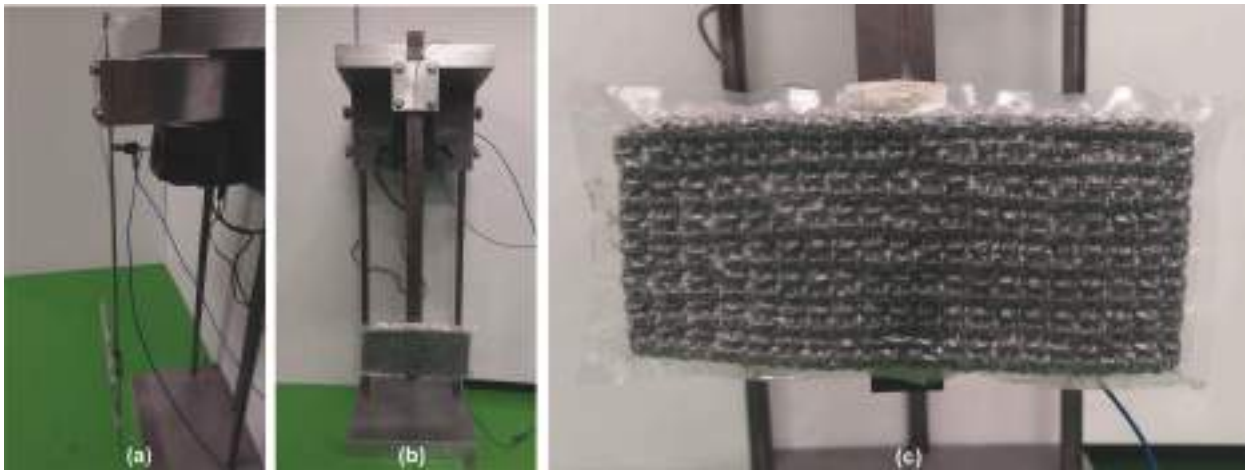

Fig. 15. Cantilever beam with the vacuum-controlled ATVA mounted at the free termination.

bending stiffness of the flapping element and hence on its fundamental resonance frequency. As discussed in Refs. [33,46,48] for shunted electro-mechanical TVAs, the online tuning can be conveniently implemented by maximising the time-averaged vibration power absorbed by the device [58], which can be measured with an impedance sensor for example. Since this study is focussed on the applicability of the proposed absorber and its vibration control performances, for simplicity, the tuning was implemented manually with a trial-and-error approach contrasting the spectra of the response of the beam without and with ATVA.

4.2. Measurement results

Fig. 16 shows the spectra of the transverse velocity at the tip of the beam per unit force excitation without ATVA (blue line) and with the ATVA suitably tuned (red line). As anticipated above, in this frequency range, the spectrum of the flexural vibration of the beam is characterised by the resonant response of the fundamental bending mode, which shows a resonance peak at about $f_1 = 38$Hz. As discussed in Section 3.2 and shown in Fig. 9, when the resonance frequency ω_a of the flapping mode of the ATVA in-vacuo beam element is closely tuned to the fundamental resonance frequency of the beam structure, the measurement shows the typical double peak spectrum [1–4]. This confirms that, indeed, the proposed vacuum-controlled ATVA generates the desired vibration absorption effect such that the response at the beam fundamental resonance frequency is significantly reduced by about 20 dB. As shown in Section 3.2, the amplitude of the two side peaks can be flattened too by raising the level of damping in the TVA. This is not feasible at this stage, although it is expected that the proposed ATVA can be equipped with a second in-vacuo adaptive beam element beam encompassing a dissipative medium given for example by a matrix structure filled with a friction powder.

To conclude, it should be highlighted that, if the ATVA were not optimally tuned, as can be deduced by the spectra of the base impedance shown in Figs. 9 and 12, the ATVA would exert a mass effect, which would lower the resonance frequency of the hosting beam structure.

5. Conclusions

This paper has investigated the vibration response of a new in-vacuo adaptive beam element for vibration control. The element is made by one or a pile of multiple structured fabric strips wrapped in a deflated bag. The structured fabrics are formed by a regular mail of interlocked truss-like unit elements. The paper has considered beam elements with a one or two mails fabricated with cubic, spherical-octahedral and octahedral grains. A practical application has been considered too, where the in-vacuo adaptive beam element has been configured with a centre post to work as an adaptive tuned vibration absorber for the control of the broad band response of a target flexural mode of a hosting beam structure.

To start with, the paper has shown that the bending stiffness of the in-vacuo adaptive beam element can be suitably varied by changing the vacuum pressure in the bag. This effect depends on the type of elementary truss grains of the fabric and on the number of layers wrapped in the bag. For instance, the cubic and octahedral fabrics offers the highest bending stiffness respectively for the single- and double-layer configurations. When the vacuum pressure is raised from 5 to 80 kPa, the stiffness of two-layers cubic fabric beam is doubled. Also, the double layer octahedral structured fabric shows 5 times higher stiffness than the single layer one.

These properties can be suitably employed to shift the resonance frequency of the fundamental flapping flexural mode of the structured fabric beam, that is, of the adaptive tuneable vibration absorber application. In this respect, the study has shown that, for 5 to 80 kPa pressure range, the resonance frequency of either the single- or double-layer vibration absorbers can be increased by 30 % to 40 %. Also, the resonance frequency of the double layer vibration absorbers is about 50 % higher than that of the single layer absorber. This suggests that rather wide tuning ranges can be achieved with designs encompassing multiple layers and different types of elementary truss grains.

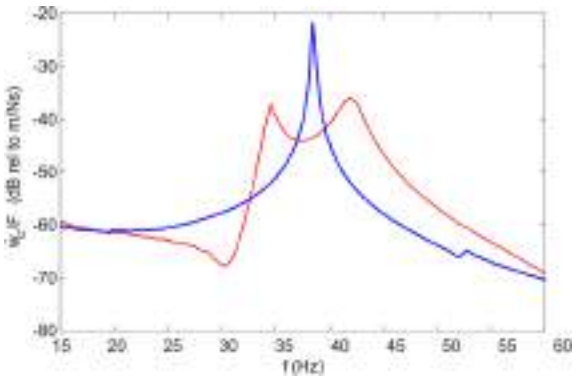

Fig. 16. Spectra of the transverse velocity at the tip of the beam per unit force excitation without (blue line) and with the vacuum-controlled ATVA suitably tuned (red line). (For interpretation of the references to colour in this figure legend, the reader is referred to the web version of this article.)

The study has also shown that the in-vacuo adaptive beam element is characterised by small vibration energy dissipation effects. For instance, the structural loss factor that does not change significantly with the vacuum level in the bag as well as with respect to the number of layers and the type of elementary grains. In general, the loss factor is comprised between 5 % and 7 %. This is a rather important feature, which indicates that the resonance frequency of the ATVA beam element can be tuned independently from the absorber damping effect. To conclude, the vacuum-controlled ATVA has been successfully implemented on a cantilever beam to control the resonant response of its fundamental bending mode, with 20 dB reductions of the peak response at resonance frequency.

CRediT authorship contribution statement

P. Gardonio: Conceptualization, Data curation, Formal analysis, Investigation, Methodology, Supervision, Validation, Visualization, Writing – original draft, Writing – review & editing. **E. Rustighi:** Conceptualization, Data curation, Formal analysis, Investigation, Methodology, Supervision, Validation, Visualization, Writing – original draft, Writing – review & editing. **S. Baldini:** Conceptualization, Data curation, Formal analysis, Investigation, Methodology, Validation, Visualization, Writing – original draft, Writing – review & editing. **C. Malacarne:** Conceptualization, Investigation, Methodology, Resources. **M. Perini:** Conceptualization, Methodology, Resources, Investigation.

Declaration of competing interest

The authors declare that they have no known competing financial interests or personal relationships that could have appeared to influence the work reported in this paper.

Acknowledgements

This work was funded by the European Union under Next Generation EU. PRIN 2022 Prot. n. 20223X5S37_001.

Data availability

Data will be made available on request.

References

[1] P. Den Hartog, Mechanical Vibrations, Fourth, McGraw-Hill, New York, 1986.
[2] J.B. Hunt, Dynamic Vibration Absorbers, Mechanical Engineering Publications Limited, London, 1979.
[3] D.J. Mead, Passive Vibration Control, John Wiley & Sons, Chichester, 1998.
[4] D.J. Inman, Engineering vibration, 4th ed., Pearson, 2013.
[5] M.A. Franchek, M.W. Ryan, R.J. Bernhard, Adaptive passive vibration control, J. Sound Vib. 189 (1996) 565–585.
[6] K. Williams, G. Chiu, R. Bernhard, Adaptive-passive absorbers using shape-memory alloys, J. Sound Vibrat. 249 (2002) 835–848.
[7] E. Rustighi, M.J. Brennan, B.R. Mace, A shape memory alloy adaptive tuned vibration absorber: design and implementation, Smart Mater. Struct. 14 (2004) 19–28, https://doi.org/10.1088/0964-1726/14/1/002.
[8] E. Rustighi, M.J. Brennan, B.R. Mace, Real-time control of a shape memory alloy adaptive tuned vibration absorber, Smart Mater. Struct. 14 (2005) 1184–1195, https://doi.org/10.1088/0964-1726/14/6/011.
[9] S. Manzoni, A. Argentino, F. Lucà, M. Berardengo, M. Vanali, SMA-based adaptive tuned mass dampers: analysis and comparison, Mech. Syst. Sig. Process. 186 (2023), https://doi.org/10.1016/j.ymssp.2022.109883.
[10] Samir B. Kumbhar, S.P. Chavan, S.S. Gawade, Adaptive tuned vibration absorber based on magnetorheological elastomer-shape memory alloy composite, Mech. Syst. Signal Process. 100 (2018) 208–223 https://doi.org/10.1016/j.ymssp.2017.07.027.
[11] Hua-xia Deng, Xing-long Gong, Lian-hua Wang, Development of an adaptive tuned vibration absorber with magnetorheological elastomer, Smart Materials and Structures, 15(5) (2006) DOI 10.1088/0964-1726/15/5/N02.

[12] F. Weber, C. Boston, M. Maślanka, An adaptive tuned mass damper based on the emulation of positive and negative stiffness with an MR damper, Smart Mater. Struct. 20 (2010) 015012, https://doi.org/10.1088/0964-1726/20/1/015012.
[13] S.B. Kumbhar, S.P. Chavan, S.S. Gawade, Adaptive tuned vibration absorber based on magnetorheological elastomer-shape memory alloy composite, Mech. Syst. Sig. Process. 100 (2018) 208–223, https://doi.org/10.1016/j.ymssp.2017.07.027.
[14] A.S. Tan, J. Aramendiz, K.H. Ross, T. Sattel, A. Fidlin, Comparative study between dry friction and electrorheological fluid switches for tuned vibration absorbers, J. Sound Vib. 460 (2019), https://doi.org/10.1016/j.jsv.2019.114874.
[15] R. Fosdick, Y. Ketema, 1998. A thermoviscoelastic dynamic vibration absorber, ASME. J. Appl. Mech. March 65(1) (1998) 17–24. https://doi.org/10.1115/1.2789023.
[16] E. Rustighi, M. Beaugrand, A viscoelastic adaptive tuned vibration absorber, The 12th Conference on Motion and Vibration MOVIC 2014, Paper 3B33, 2014 (The Japan Society of Mechanical Engineers).
[17] P. Bonello, K.H. Groves, Vibration control using a beam-like adaptive tuned vibration absorber with an actuator-incorporated mass element, Proc. Inst. Mech. Eng. C J. Mech. Eng. Sci. 223 (7) (2009) 1555–1567, https://doi.org/10.1243/09544062JMES1301.
[18] M.R.F. Kidner, M.J. Brennan, Varying the stiffness of a beam-like neutralizer under fuzzy logic control, ASME. J. Vib. Acoust 124(1) (2001) 90–99. https://doi.org/10.1115/1.1423634.
[19] P.L. Walsh, J.S. Lamancusa, A variable stiffness vibration absorber for minimization of transient vibrations, J. Sound Vib. 158 (1992) 195–211.
[20] P. Bonello, M.J. Brennan, S.J. Elliott, Vibration control using an adaptive tuned vibration absorber with a variable curvature stiffness element, Smart Mater. Struct. 14 (2005) 1055–1065.
[21] D. Niederberger, S. Behrens, A.J. Fleming, S.O.R. Moheimani, M. Morari, Adaptive electromagnetic shunt damping, IEEE/ASME Trans. Mechatron. 11 (2006) 103–108, https://doi.org/10.1109/tmech.2005.859844.
[22] A.J. Fleming, S.O.R. Moheimani, Inertial vibration control using a shunted electromagnetic transducer, IEEE/ASME Trans. Mechatron. 11 (2006) 84–92, https://doi.org/10.1109/tmech.2005.863364.
[23] Christoph Paulitsch, Paolo Gardonio, S.J. Elliott, Active vibration damping using an inertial electrodynamic actuator, J. Vib. Acoust. 129 (2007) 39–47.
[24] T. Inoue, Y. Ishida, M. Sumi, Vibration suppression using electromagnetic resonant shunt damper, J. Vib. Acoust. 130 (2008), https://doi.org/10.1115/1.2889916.
[25] R. Palomera-Arias, J.J. Connor, J.A. Ochsendorf, Feasibility study of passive electromagnetic damping systems, J. Struct. Eng. 134 (2008) 164–170, https://doi.org/10.1061/(asce)0733-9445(2008)134:1(164).
[26] T.-H. Cheng, I.-K. Oh, A current-flowing electromagnetic shunt damper for multi-mode vibration control of cantilever beams, Smart Mater. Struct. 18 (2009) 095036, https://doi.org/10.1088/0964-1726/18/9/095036.
[27] X. Zhang, H. Niu, B. Yan, A novel multimode negative inductance negative resistance shunted electromagnetic damping and its application on a cantilever plate, J. Sound Vib. 331 (2012) 2257–2271, https://doi.org/10.1016/j.jsv.2011.12.028.
[28] A.J. McDaid, B.R. Mace, A self-tuning electromagnetic vibration absorber with adaptive shunt electronics, Smart Mater. Struct. 22 (2013) 105013, https://doi.org/10.1088/0964-1726/22/10/105013.
[29] B. Yan, X. Zhang, Y. Luo, Z. Zhang, S. Xie, Y. Zhang, Negative impedance shunted electromagnetic absorber for broadband absorbing: experimental investigation, Smart Mater. Struct. 23 (2014) 125044, https://doi.org/10.1088/0964-1726/23/12/125044.
[30] A.J. McDaid, B.R. Mace, A robust adaptive tuned vibration absorber using semi-passive shunt electronics, IEEE Trans. Ind. Electron. 63 (2016).
[31] E. Turco, P. Gardonio, Sweeping shunted electro-magnetic tuneable vibration absorber: design and implementation, J. Sound Vib. 407 (2017) 82–105, https://doi.org/10.1016/j.jsv.2017.06.035.
[32] E. Turco, P. Gardonio, R. Petrella, L. Dal Bo, Modular vibration control unit formed by an electromagnetic proof-mass transducer and sweeping resistive-inductive shunt, J. Vib. Acoust. 142 (2020), https://doi.org/10.1115/1.4047068.
[33] P. Gardonio, E. Turco, A. Kras, L.D. Bo, D. Casagrande, Semi-active vibration control unit tuned to maximise electric power dissipation, J. Sound Vib. 499 (2021) 116000, https://doi.org/10.1016/j.jsv.2021.116000.
[34] X.i. Wang, Wu. Haomin, B. Yang, Micro-vibration suppressing using electromagnetic absorber and magnetostrictive isolator combined platform, Mech. Syst. Sig. Process. 139 (2020), https://doi.org/10.1016/j.ymssp.2019.106606.
[35] Tobias Greve Larsen, Zili Zhang, Jan Høgsberg, Vibration damping of an offshore wind turbine by optimally calibrated pendulum absorber with shunted electromagnetic transducer, J. Sound Vibration 505 (2021) https://doi.org/10.1016/j.jsv.2021.116144.
[36] S. Wu, Piezoelectric shunts with a parallel R-L circuit for structural damping and vibration control, SPIE Proc. (1996), https://doi.org/10.1117/12.239093.
[37] N.W. Hagood, A. von Flotow, Damping of structural vibrations with piezoelectric materials and passive electrical networks, J. Sound Vib. 146 (1991) 243–268, https://doi.org/10.1016/0022-460x(91)90762-9.
[38] J.J. Hollkamp, T.F. Starchville, A self-tuning piezoelectric vibration absorber, J. Intell. Mater. Syst. Struct. 5 (1994) 559–566, https://doi.org/10.1177/1045389x9400500412.
[39] Christopher L. Davis, George A. Lesieutre, An actively tuned solid-state vibration absorber using capacitive shunting of piezoelectric stiffness, J. Sound Vibrat. 232(3) (2000) 601–617.
[40] A.J. Fleming, S.O.R. Moheimani, Adaptive piezoelectric shunt damping, Smart Mater. Struct. 12 (2003) 36–48, https://doi.org/10.1088/0964-1726/12/1/305.
[41] D. Niederberger, A. Fleming, S.O.R. Moheimani, M. Morari, Adaptive multi-mode resonant piezoelectric shunt damping, Smart Mater. Struct. 13 (2004) 1025–1035, https://doi.org/10.1088/0964-1726/13/5/007.
[42] O. Thomas, J. Ducarne, J.-F. Deü, Performance of piezoelectric shunts for vibration reduction, Smart Mater. Struct. 21 (2012) 015008, https://doi.org/10.1088/0964-1726/21/1/015008.
[43] N. Alujević, I. Tomac, P. Gardonio, Tuneable vibration absorber using acceleration and displacement feedback, J. Sound Vib. 331 (2012) 2713–2728, https://doi.org/10.1016/j.jsv.2012.01.012.
[44] P. Gardonio, D. Casagrande, Shunted piezoelectric patch vibration absorber on two-dimensional thin structures: tuning considerations, J. Sound Vib. 395 (2017) 26–47, https://doi.org/10.1016/j.jsv.2017.02.019.
[45] P. Gardonio, M. Zientek, L. Dal Bo, Panel with self-tuning shunted piezoelectric patches for broadband flexural vibration control, Mech. Syst. Sig. Process. 134 (2019) 106299, https://doi.org/10.1016/j.ymssp.2019.106299.
[46] P. Gardonio, G. Konda Rodrigues, L. Dal Bo, E. Turco, Extremum seeking online tuning of a piezoelectric vibration absorber based on the maximisation of the shunt electric power absorption, Mech. Syst. Sig. Process. 176 (2022) 109171, https://doi.org/10.1016/j.ymssp.2022.109171.
[47] J. Høgsberg, Vibration control by piezoelectric proof-mass absorber with resistive-inductive shunt, Mech. Adv. Mater. Struct. 28 (2019) 141–153, https://doi.org/10.1080/15376494.2018.1551587.
[48] G. Konda Rodrigues, P. Gardonio, L. Dal Bo, E. Turco, Piezoelectric patch vibration control unit connected to a self-tuning RL-shunt set to maximise electric power absorption, J. Sound Vib. 536 (2022) 117154, https://doi.org/10.1016/j.jsv.2022.117154.
[49] Zein A. Shami, Christophe Giraud-Audine, Olivier Thomas, A nonlinear piezoelectric shunt absorber with a 2:1 internal resonance: Theory, Mechanical Systems and Signal Processing, Volume 170, 2022, https://doi.org/10.1016/j.ymssp.2021.108768.
[50] L. Dal Bo, P. Gardonio, D.E. Casagrande, S. Saggini, Smart panel with sweeping and switching piezoelectric patch vibration absorbers: experimental results, Mech. Syst. Sig. Process. 120 (2019) 308–325, https://doi.org/10.1016/j.ymssp.2018.10.024.
[51] M.J. Brennan and N.S. Ferguson. Vibration Control, in: F. Fahy, J. Walker (Eds.), Advanced Applications in Acoustics, Noise and Vibration, CRC Press, London, 2004, pp. 530–580.
[52] S.H. Crandall, W.D. Mark, Random Vibration in Mechanical Systems, Academic Press, London, 1963.
[53] G.B. Warburton, Optimum absorber parameters for various combinations of response and excitation parameters, Earthq. Eng. Struct. Dyn. 10 (1982) 381–401, https://doi.org/10.1002/eqe.4290100304.

[54] Y. Iwata, On the construction of the dynamic vibration absorber, Jpn. Soc. Mech. Eng. 820 (1982) 150–152.
[55] O. Nishihara, T. Asami, Closed-form solutions to the exact optimizations of dynamic vibration absorbers (minimizations of the maximum amplitude magnification factors), J. Vib. Acoust. 124 (2002) 576–582, https://doi.org/10.1115/1.1500335.
[56] S. Krenk, J. Høgsberg, Equal modal damping design for a family of resonant vibration control formats, J. Vib. Control 19 (2012) 1294–1315, https://doi.org/10.1177/1077546312446796.
[57] S. Krenk, J. Høgsberg, Tuned mass absorber on a flexible structure, J. Sound Vib. 333 (2014) 1577–1595, https://doi.org/10.1016/j.jsv.2013.11.029.
[58] M. Zilletti, S.J. Elliott, E. Rustighi, Optimisation of dynamic vibration absorbers to minimise kinetic energy and maximise internal power dissipation, J. Sound Vib. 331 (2012) 4093–4100, https://doi.org/10.1016/j.jsv.2012.04.023.
[59] S. Baldini, P. Gardonio, E. Rustighi, C. Malacarne, M. Perini, In-vacuo structured fabric tuneable vibration absorber, in: ECCOMAS Proceedia, 2023.
[60] J.C. Snowdon, M.A. Nobile, Beamlike dynamic vibration absorbers, Acust. 44 (1980) 98–108.
[61] J.C. Snowdon, A.A. Wolfe, R.L. Kerlin, The cruciform dynamic vibration absorber, J. Acoust. Soc. Am. 75 (6) (1984) 1792–1799.
[62] R.T. Faal, M.B. Amiri, A.A. Pirmohammadi,·A.S. Milani, Vibration analysis of undamped, suspended multi-beam absorber systems Meccanica 47 (2012) 1059–1078 DOI 10.1007/s11012-011-9493-2.
[63] T. Aida, S. Toda, N. Ogawa, Y. Imada, Vibration control of beams by beam-type dynamic vibration absorbers, J. Eng. Mech. 118 (2) (1992) 248–258.
[64] Karina M. Tsuruta, Domingos A. Rade, Roberto M. Finzi Neto, Aldemir A. Cavalini, Experimental evaluation of a cruciform piezoelectric energy harvester, Mech. Syst. Signal Process. 79 (2016) 141–148, https://doi.org/10.1016/j.ymssp.2016.03.005.
[65] I. Gibson, D. Rosen, B. Stucker, Additive Manufacturing Technologies : 3D Printing, Rapid Prototyping, and Direct Digital Manufacturing, Springer New York, New York, Ny, 2015.
[66] L.W. Xiaogang Chen, L.-J. Taylor, An overview on fabrication of three-dimensional woven textile preforms for composites, Text. Res. J. 81 (2011) 932–944, https://doi.org/10.1177/0040517510392471.
[67] K. Cherenack, C. Zysset, T. Kinkeldei, N. Münzenrieder, G. Tröster, Woven electronic fibers with sensing and display functions for smart textiles, Adv. Mater. 22 (2010) 5178–5182, https://doi.org/10.1002/adma.201002159.
[68] F. Boussu, I. Cristian, S. Nauman, General definition of 3D warp interlock fabric architecture, Compos. B Eng. 81 (2015) 171–188, https://doi.org/10.1016/j.compositesb.2015.07.013.
[69] J. Engel, C. Liu, Creation of a metallic micromachined chain mail fabric, J. Micromech. Microeng. 17 (2007) 551–556, https://doi.org/10.1088/0960-1317/17/3/018.
[70] M.A. Wijnhoven, A. Moskvin, Digital replication and reconstruction of mail armour, J. Cult. Herit. (2020), https://doi.org/10.1016/j.culher.2020.04.010.
[71] Y. Wang, L. Li, D. Hofmann, J.E. Andrade, C. Daraio, Structured fabrics with tunable mechanical properties, Nature 596 (2021) 238–243, https://doi.org/10.1038/s41586-021-03698-7.
[72] A.J. Liu, S.R. Nagel, Jamming is not just cool any more, Nature 396 (1998) 21–22, https://doi.org/10.1038/23819.
[73] D. Levine, Jamming and the statics of granular materials, Jamming Rheol.: Constrained Dyn. Microscopic Macroscopic Scales (2001) 9.
[74] A.J. Liu, S.R. Nagel, Jamming and rheology: constrained dynamics on microscopic and macroscopic scales, Taylor & Francis, London, 2001.
[75] C.S. O'Hern, L.E. Silbert, Jamming at zero temperature and zero applied stress: the epitome of disorder, Phys. Rev. E 68 (2003).
[76] M. van Hecke, Jamming of soft particles: geometry, mechanics, scaling and isostaticity, J. Phys. Condens. Matter 22 (2009) 033101, https://doi.org/10.1088/0953-8984/22/3/033101.
[77] A.J. Liu, S.R. Nagel, The jamming transition and the marginally jammed solid, Annu. Rev. Condens. Matter Phys. 1 (2010) 347–369, https://doi.org/10.1146/annurev-conmatphys-070909-104045.
[78] D. Bi, J. Zhang, B. Chakraborty, R.P. Behringer, Jamming by shear, Nature 480 (2011) 355–358, https://doi.org/10.1038/nature10667.
[79] H.M. Jaeger, Celebrating Soft Matter's 10th Anniversary: toward jamming by design, Soft Matter 11 (2015) 12–27, https://doi.org/10.1039/c4sm01923g.
[80] R.P. Behringer, B. Chakraborty, The physics of jamming for granular materials: a review, Rep. Prog. Phys. 82 (2018) 012601.
[81] H.M. Jaeger, S.R. Nagel, R.P. Behringer, The physics of granular materials, Phys. Today 49 (1996) 32–38, https://doi.org/10.1063/1.881494.
[82] T.S. Majmudar, R.P. Behringer, Contact force measurements and stress-induced anisotropy in granular materials, Nature 435 (2005) 1079–1082, https://doi.org/10.1038/nature03805.
[83] R. Hurley, S.A. Hall, J.E. Andrade, J.P. Wright, Quantifying interparticle forces and heterogeneity in 3D granular materials, Phys. Rev. Lett. 117 (2016), https://doi.org/10.1103/physrevlett.117.098005.
[84] M. Arman Pazouki, K. Kwarta, W.J. Williams, R. Likos, P. Serban, D.N. Jayakumar, Compliant contact versus rigid contact: a comparison in the context of granular dynamics, Phys. Rev. 96 (2017), https://doi.org/10.1103/physreve.96.042905.
[85] L. Li, E. Marteau, J.E. Andrade, Capturing the inter-particle force distribution in granular material using LS-DEM, Granul. Matter 21 (2019), https://doi.org/10.1007/s10035-019-0893-7.
[86] A.V. Dyskin, Y. Estrin, A.J. Kanel-Belov, E. Pasternak, A new concept in design of materials and structures: assemblies of interlocked tetrahedron-shaped elements, Scr. Mater. 44 (2001) 2689–2694, https://doi.org/10.1016/s1359-6462(01)00968-x.
[87] A.V. Dyskin, E. Pasternak, Y. Estrin, Mortarless structures based on topological interlocking, Front. Struct. Civil Eng. (2012) 188–197, https://doi.org/10.1007/s11709-012-0156-8.
[88] C.S. O'Hern, L.E. Silbert, A.J. Liu, S.R. Nagel, Jamming at zero temperature and zero applied stress: the epitome of disorder, Phys. Rev. E 68 (2003), https://doi.org/10.1103/physreve.68.011306.
[89] L.E. Silbert, A.J. Liu, S.R. Nagel, Structural signatures of the unjamming transition at zero temperature, Phys. Rev. E 73 (2006), https://doi.org/10.1103/physreve.73.041304.
[90] C. Heussinger, J.-L. Barrat, Jamming transition as probed by quasistatic shear flow, Phys. Rev. Lett. 102 (2009), https://doi.org/10.1103/physrevlett.102.218303.
[91] D. Vågberg, P. Olsson, S. Teitel, Glassiness, rigidity, and jamming of frictionless soft core disks, Phys. Rev. E 83 (2011), https://doi.org/10.1103/physreve.83.031307.
[92] H.A. Makse, D.W. Johnson, L.B. Schwartz, Packing of compressible granular materials, Phys. Rev. Lett. 84 (2000) 4160–4163, https://doi.org/10.1103/physrevlett.84.4160.
[93] L.E. Silbert, Jamming of frictional spheres and random loose packing, Soft Matter 6 (2010) 2918, https://doi.org/10.1039/c001973a.
[94] J. Zhang, T.S. Majmudar, A. Tordesillas, R.P. Behringer, Statistical properties of a 2D granular material subjected to cyclic shear, Granul. Matter 12 (2010) 159–172, https://doi.org/10.1007/s10035-010-0170-2.
[95] M. Otsuki, H. Hayakawa, Critical scaling near jamming transition for frictional granular particles, Phys. Rev. E 83 (2011), https://doi.org/10.1103/physreve.83.051301.
[96] R. Pastore, M.P. Ciamarra, A. Coniglio, "Flow and jam" of frictional athermal systems under shear stress, Phil. Mag. 91 (2011) 2006–2013, https://doi.org/10.1080/14786435.2010.540457.
[97] J. Ren, J.A. Dijksman, R.P. Behringer, Reynolds pressure and relaxation in a sheared granular system, Phys. Rev. Lett. 110 (2013), https://doi.org/10.1103/physrevlett.110.018302.
[98] S. Sarkar, D. Bi, J. Zhang, R.P. Behringer, B. Chakraborty, Origin of rigidity in dry granular solids, Phys. Rev. Lett. 111 (2013), https://doi.org/10.1103/physrevlett.111.068301.
[99] S. Sarkar, B. Chakraborty, Shear-induced rigidity in athermal materials: a unified statistical framework, Phys. Rev. E 91 (2015), https://doi.org/10.1103/physreve.91.042201.
[100] M.E. Cates, J.P. Wittmer, Jean-Philippe Bouchaud, Philippe Claudin, Jamming, Force Chains, and Fragile Matter, Physical Review Letters. 81 (1998) 1841–1844.

[101] A.G. Athanassiadis, M.Z. Miskin, P.D. Kaplan, N. Rodenberg, S.H. Lee, J. Merritt, E. Brown, J.R. Amend, H. Lipson, H.M. Jaeger, Particle shape effects on the stress response of granular packings, Soft Matter 10 (2014) 48–59, https://doi.org/10.1039/c3sm52047a.
[102] S. Torquato, Y. Jiao, Organizing principles for dense packings of nonspherical hard particles: not all shapes are created equal, Phys. Rev. E 86 (2012), https://doi.org/10.1103/physreve.86.011102.
[103] A. Wouterse, S.R. Williams, A.P. Philipse, Effect of particle shape on the density and microstructure of random packings, J. Phys. Condens. Matter 19 (2007) 406215, https://doi.org/10.1088/0953-8984/19/40/406215.
[104] J. Zhao, S. Li, P. Lu, L. Meng, T. Li, H. Zhu, Shape influences on the packing density of frustums, Powder Technol. 214 (2011) 500–505, https://doi.org/10.1016/j.powtec.2011.09.013.
[105] H.F. Burcharth, K. d'Angremond, J.W. van der Meer, Z. Liu, Empirical formula for breakage of dolosse and tetrapods, Coast. Eng. 40 (2000) 183–206, https://doi.org/10.1016/s0378-3839(00)00010-7.
[106] S. Rémond, J.L. Gallias, A. Mizrahi, Simulation of the packing of granular mixtures of non-convex particles and voids characterization, Granul. Matter 10 (2008) 157–170, https://doi.org/10.1007/s10035-007-0082-y.
[107] V.V. Iryna Malinouskaya, J.-F. Mourzenko, P.M. Adler, Random packings of spiky particles: geometry and transport properties, Phys. Rev. E 80 (2009), https://doi.org/10.1103/physreve.80.011304.
[108] J. de Graaf, R. van Roij, M. Dijkstra, Dense regular packings of irregular nonconvex particles, Phys. Rev. Lett. 107 (2011), https://doi.org/10.1103/physrevlett.107.155501.
[109] N. Gravish, S.V. Franklin, D.L. Hu, D.I. Goldman, Entangled granular media, Phys. Rev. Lett. 108 (2012), https://doi.org/10.1103/physrevlett.108.208001.
[110] F. Ludewig, N. Vandewalle, Strong interlocking of nonconvex particles in random packings, Phys. Rev. E 85 (2012), https://doi.org/10.1103/physreve.85.051307.
[111] Baptiste Saint-Cyr, Jean-Yves Delenne, C. Voivret, Farhang Radjaï, Philippe Sornay, Rheology of granular materials composed of nonconvex particles, Phys. Rev. E. 84 (2011). https://doi.org/10.1103/physreve.84.041302.
[112] E. Brown, A. Nasto, A.G. Athanassiadis, H.M. Jaeger, Strain stiffening in random packings of entangled granular chains, Phys. Rev. Lett. 108 (2012), https://doi.org/10.1103/physrevlett.108.108302.
[113] L.-N. Zou, X. Cheng, M.L. Rivers, H.M. Jaeger, S.R. Nagel, The packing of granular polymer chains, Science 326 (2009) 408–410, https://doi.org/10.1126/science.1177114.
[114] P. Gardonio, M.J. Brennan. Mobility and impedance methods in structural dynamics, in: F. Fahy, J. Walker (Eds.), Advanced Applications in Acoustics, Noise and Vibration, CRC Press, London, 2004, pp. 389–447.
[115] K. Shin, J.K. Hammond, Fundamentals of Signal Processing for Sound and Vibration Engineers, John Wiley & Sons Ltd, Chichester, 2008.
[116] F.J. Fahy, Paolo Gardonio, Academic Press, Oxford, Sound and Structural Vibration, 2007.
[117] W.T. Thomson, Theory of vibration with applications, Fourth Edition, CRC Press Taylor & Francis Group, 2017.